DALTON
FULL PAPER

Combination of crystal-field dependent and independent paramagnetic NMR hyperfine shift analysis methods for investigating the solution structures of inert self-assembled heterodimetallic d–f supramolecular complexes†

Stéphane Rigault,[a] Claude Piguet,[a]* Gérald Bernardinelli[b] and Gérard Hopfgartner[c]

[a] *Department of Inorganic, Analytical and Applied Chemistry, University of Geneva, 30 quai E. Ansermet, CH-1211 Geneva 4, Switzerland. E-mail: Claude.Piguet@chiam.unige.ch*
[b] *Laboratory of X-ray Crystallography, 24 quai E. Ansermet, CH-1211 Geneva 4, Switzerland*
[c] *F. Hoffmann-La Roche Ltd, Pharmaceuticals Division, PRNS 68/142, CH-4070 Basle, Switzerland*

Received 6th September 2000, Accepted 18th October 2000
First published as an Advance Article on the web 4th December 2000

The segmental ligand 2-{6-[*N*,*N*-diethylcarbamoyl]-pyridin-2-yl}-1,1′-dimethyl-2′-(5-methylpyridin-2-yl)-5,5′-methylenebis[1*H*-benzimidazole] (L) produces quantitatively the self-assembled triple-stranded non-covalent head-to-head-to-head podates (HHH)-[$LnCo^{II}L_3$]$^{5+}$ (Ln = La to Lu or Y) in acetonitrile. Subsequent selective $Co^{II/III}$ oxidation gives the related rigid supramolecular complexes (HHH)-[$LnCo^{III}L_3$]$^{6+}$ possessing an inert and diamagnetic pseudo-octahedral cobalt(III) tripod ideally suited for testing and extending paramagnetic NMR hyperfine shift analysis methods in solution for dimetallic complexes. Comparison of structure independent NMR hyperfine shift analysis methods led to the conclusion that only a combination of both crystal-field independent and dependent approaches is suitable for (i) accurately separating contact and pseudo-contact contributions in axial complexes, (ii) rationalising and predicting NMR spectra for (HHH)-[$LnCo^{III}L_3$]$^{6+}$ and (iii) investigating spin delocalisation and isostructurality along the lanthanide series in solution. The extraction of molecular structures in solution from pseudo-contact terms by using linear and non-linear least-squares fits of lanthanide induced shifts (LIS) and field-dependent lanthanide induced relaxation (LIR) effects demonstrates that the crystal structures of the cations (HHH)-[$LnCo^{III}L_3$]$^{6+}$ in [$LaCo^{III}(L)_3$][ClO_4]$_{5.5}$[OH]$_{0.5}$·$4CH_3CN$·$2(H_2O)$ and [$LuCo^{III}(L)_3$][CF_3SO_3]$_6$·$2CH_3CN$·H_2O are maintained in acetonitrile, thus confirming the considerable rigidity of these supramolecular assemblies. An extension of this complete NMR approach for the characterisation of (HHH)-[$LnCo^{II}(L)_3$]$^{5+}$ in which both metal ions are strongly paramagnetic provides identical conclusions for magnetically uncoupled dimetallic systems, thus opening new perspectives for the characterisation of polymetallic d–f supramolecular complexes in solution. The origin of the systematic breaks occurring near the middle of the lanthanide series for classical structure independent hyperfine shift analysis methods is discussed.

Introduction

It is now well established that thermodynamic self-assembly involving metal ions and ligands requires labile co-ordination bonds in order completely to explore the energy hypersurface, thus leading to defect-free, self-healing and organised metallo-supramolecular assemblies.[1,2] As a result of their strong, but labile dative bonds with nitrogen-donor ligands, much effort has been focused on the introduction of 3d-block ions into polymetallic helicates,[3] racks and grids,[4] boxes,[5] catenates,[6] metallacrowns,[7] clusters[8] and cylinders[9] whose structures in solution are rigid enough to be characterised by resonance techniques (NMR or EPR).[1,2] The increased covalence between nitrogen donors and 4d-block (Pd^{II}) and especially 5d-block ions (Pt^{II}) strongly limits lability and reversibility[10] and harsh conditions (high temperatures and ionic strengths) are required to overcome the kinetic barriers of the assembly process,[5] but the final diamagnetic and inert architectures are particularly easy to characterise by NMR in solution. Lanthanide ions, Ln^{III}, display opposite behaviours because their considerable labilities and lack of pronounced stereochemical preferences often prevent the formation of rigid and well defined self-assembled complexes.[11] Strategies based on suitable preorganisation and/or predisposition of the receptor may overcome these limitations as exemplified by (i) the branched macrocyclic 1,4,7,10-tetraazacyclododecane-*N*,*N*′,*N*″,*N*‴-tetraacetate (DOTA)[12] and its derivatives [13] which give highly stable and kinetically inert complexes [Ln(DOTA)]$^-$ working as tuneable MRI contrast agents (Ln = Gd),[14] (ii) covalent heterodimetallic d–f podates[15] and (iii) acyclic f–f triple-stranded helicates.[16] In all cases, Ln^{III} are efficiently encapsulated within the receptors which provides rigid and inert complexes suitable for their unambiguous characterisation by using paramagnetic NMR techniques in solution. For [Ln(DOTA)]$^-$, a detailed structural analysis shows the presence of two inert structural isomers on the NMR timescale corresponding to normal and inverted monocapped square antiprisms whose relative ratios vary along the lanthanide series.[17] However, each isomer produces an isostructural series from La^{III} to Lu^{III} according to the classical approach (see eqns. 4, 5).[17] A related analysis for semi-rigid

---

† Electronic supplementary information (ESI) available: tables of molecular peaks obtained by ESI-MS, longitudinal and transverse relaxation times, axial paramagnetic anisotropies and axial co-ordinates for (HHH)-[$LnCo^{III}L_3$]$^{6+}$ in acetonitrile; tables of least-squares planes and structural data for **6** and **7**; table of geometric factors R_{ik} and intercepts $F_i' - F_k' R_{ik}$ for (HHH)-[$LnCo^{II}(L)_3$]$^{5+}$ in acetonitrile; figures showing packing in **7**, linear plots of relaxation rates *versus* the square of magnetic fields for (HHH)-[$LnCo^{II}L_3$]$^{6+}$ and a plot of $\Delta_{ij}/\langle S_z\rangle_j$ *vs.* $\Delta_{kj}/\langle S_z\rangle_j$ for H^{12}–H^{13} in (HHH)-[$LnCo^{II}L_3$]$^{5+}$ in acetonitrile. See http://www.rsc.org/suppdata/dt/b0/b007219m/

DOI: 10.1039/b007219m

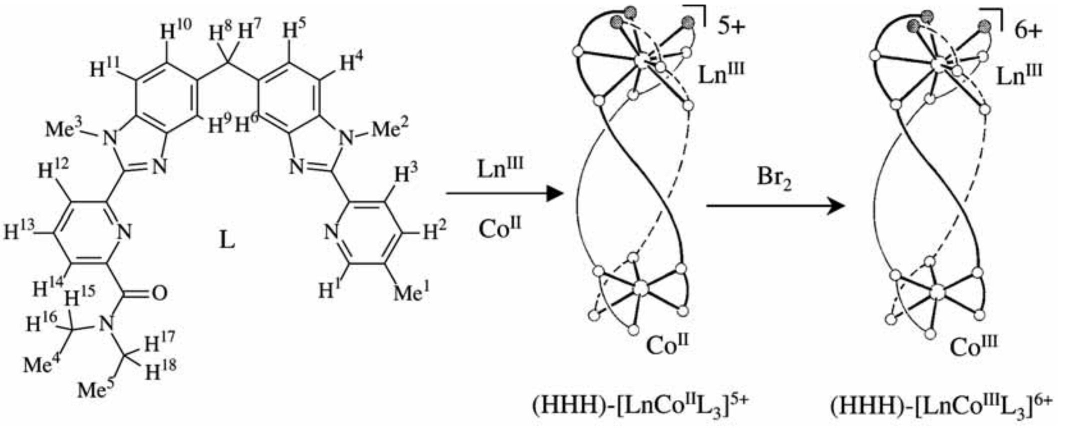

Fig. 1 Self-assembly with post-modification of the inert non-covalent podate (HHH)-$[\mathrm{LnCo^{III}L_3}]^{6+}$ in acetonitrile.

homodimetallic lanthanide-containing triple-stranded helicates is compatible with the existence of a single species in solution, but exhibiting a geometrical change in the middle of the series.[16c] A recent reinvestigation of these helicates by using a crystal-field independent technique (see eqn. 6) reaches different conclusions,[18,19] and more rigid systems are thus required to support this new approach for characterising polymetallic lanthanide-containing assemblies. During the last few years we have launched a research programme aiming at the design of semi-rigid self-assembled non-covalent (head-to-head-to-head) podates (HHH)-$[\mathrm{LnML_3}]^{5+}$ (Ln = La to Lu; M = Fe[20] or Zn[21]) in which the pseudo-octahedral d-block tripod ensures a facial arrangement of the three tridentate binding units for their facial co-ordination around $\mathrm{Ln^{III}}$ (Fig. 1). Remarkable luminescent and magnetic properties have been evidenced, but a precise structural characterisation in solution by paramagnetic NMR is precluded by significant deviations of classical methods from linearity.[21] In order to prepare lanthanide-containing podates which are rigid enough quantitatively to address the effects of crystal-field parameters, hyperfine coupling constants and structural changes on the paramagnetic NMR data, we have introduced inert $\mathrm{Co^{III}}$ ($\mathrm{d^6}$ low spin)[10] into the tripod. (HHH)-$[\mathrm{LnCo^{II}L_3}]^{5+}$ is selectively obtained by a self-assembly process which takes advantage of the lability of the reduced precursor $\mathrm{Co^{II}}$ ($\mathrm{d^7}$ high spin),[10] while subsequent oxidation gives (HHH)-$[\mathrm{LnCo^{III}L_3}]^{6+}$ (Fig. 1).[22]

Preliminary investigations[19] of the solution structure of (HHH)-$[\mathrm{LnCo^{III}L_3}]^{6+}$ show that the C_3-symmetrical triple helical structure is maintained along the complete lanthanide series and that crystal-field effects are responsible for the breaks (= abrupt deviations from linearity)[17] observed according to the classical approach (see eqns. 4 and 5). Moreover, reliable predictions of NMR spectra for strongly paramagnetic podates (HHH)-$[\mathrm{LnCo^{III}L_3}]^{6+}$ (Ln = Tb to Er) are only accessible with crystal-field independent hyperfine shift analysis methods.[23] This system is thus ideally suited for further developments of paramagnetic NMR techniques and we report in this paper a thorough description of the thermodynamic self-assembly process with post-modification producing the inert lanthanide-containing supramolecular podates (HHH)-$[\mathrm{LnCo^{III}L_3}]^{6+}$ whose ^{1}H NMR LIS (Lanthanide-Induced Shifts) and LIR (Lanthanide-Induced Relaxation) allow quantitative correlation between crystal and solution structures. Extension of this approach for electronic and structural characterisation of (HHH)-$[\mathrm{LnCo^{II}L_3}]^{5+}$ containing two different paramagnetic centres opens new perspectives for investigating polymetallic d–f complexes in solution.

Theory

The isotropic paramagnetic NMR shift Δ_{ij} induced at a nucleus i in a monometallic axial complex (*i.e.* possessing at least a C_3 axis)[24] by a lanthanide j is given by eqn. (1) in which δ_{ij} is the

$$\Delta_{ij} = \delta_{ij} - \delta_i^{\mathrm{dia}} = \delta_{ij}^{\mathrm{c}} + \delta_{ij}^{\mathrm{pc}} = F'_i\langle S_z\rangle_j + G'_iA_2^0\langle r^2\rangle C_j \qquad (1)$$

observed NMR shift, δ_i^{dia} the diamagnetic contribution (given by the NMR shift of the related complexes with Ln = La, Y or Lu), δ_{ij}^{c} the paramagnetic contact shift (associated with through-bond Fermi interactions)[25] and $\delta_{ij}^{\mathrm{pc}}$ the paramagnetic pseudo-contact shift (associated with the residual through-space dipolar interaction).[26] The last two contributions can be developed according to classical theory which considers $\mathrm{Ln^{III}}$ as a paramagnetic dot with minor spin delocalisation.[17] $\langle S_z\rangle_j$ is the projection of the total electron spin magnetisation of the lanthanide j onto the direction of the external magnetic field,[25] C_j a magnetic constant at a given temperature T measuring the second-order magnetic axial anisotropy of the paramagnetic lanthanide j (Bleaney's factor)[26] which was scaled to -100 for Dy and $A_2^0\langle r^2\rangle$ the axial crystal-field parameter which measures the magnitude of the interaction between a given lanthanide j and the ligand donor atoms. F'_i is proportional to the electron–nuclear hyperfine coupling constant (A_i, eqn. 2) and G'_i to the

$$F'_i = \frac{\delta_{ij}^{\mathrm{c}}}{\langle S_z\rangle_j} = \frac{F_i}{T} = \frac{1}{T}\cdot\frac{A_i}{\hbar\gamma B_0} \qquad (2)$$

geometric factor $(1 - 3\cos^2\theta_i)/r_i^3$ of nucleus i that contains the structural information about the complex (eqn. 3; θ_i is the angle

$$G'_i = \frac{\delta_{ij}^{\mathrm{pc}}}{A_2^0\langle r^2\rangle C_j} = \frac{G_i}{T^2} = \frac{1}{T^2}\cdot\frac{1 - 3\cos^2\theta_i}{r_i^3} \qquad (3)$$

between the Ln–(nucleus i) vector and the main axis (z axis) of the magnetic susceptibility tensor of the complex (*i.e.* the main molecular symmetry axis in axial complexes with at least a threefold symmetry)[24] and r_i is the Ln–(nucleus i) distance). F'_i and G'_i depend only on the topological and geometrical location of the nucleus i and their specific dependences on the temperature[27] have tentatively been used to separate contact and pseudo-contact contributions with only poor accuracy[28,29] as a result of (i) the limited temperature range accessible in solution and (ii) the complicated dependence of $\langle S_z\rangle_j$[25] and C_j[26] on temperature. We have thus fixed the temperature at 298 K for all measurements and used the temperature independent equation (1).

Eqns. (4) and (5) correspond to the linear forms of eqn. (1) which are used for testing isostructurality along the lanthanide

$$\frac{\Delta_{ij}}{\langle S_z\rangle_j} = F'_i + G'_iA_2^0\langle r^2\rangle\cdot\frac{C_j}{\langle S_z\rangle_j} \qquad (4)$$

$$\frac{\Delta_{ij}}{C_j} = F'_i\cdot\frac{\langle S_z\rangle_j}{C_j} + G'_iA_2^0\langle r^2\rangle \qquad (5)$$

series according to (i) $\langle S_z \rangle_j$[25] and C_j[26] terms tabulated for the free ions are satisfying approximations of their experimental values in the homogeneous series of lanthanide complexes and (ii) F_i' and $A_2^0\langle r^2 \rangle$ are constant along the series. Any deviation of the plots $\Delta_{ij}/\langle S_z \rangle_j$ *vs.* $C_j/\langle S_z \rangle_j$ (eqn. 4) or Δ_{ij}/C_j *vs.* $\langle S_z \rangle_j/C_j$ (eqn. 5) from linearity for a given nucleus i along the lanthanide series under these conditions is thus interpreted as a structural change which affects G_i'.[30]

Recent results for macrocyclic[31,32] and acyclic[19,23] axial lanthanide complexes have established that $A_2^0\langle r^2 \rangle$ and/or F_i' may vary along the lanthanide series without implying major structural changes which precludes the straightforward interpretation of eqns. (4) and (5). The simultaneous consideration of two nuclei i and k within the same axial complex allows removal of the magnetic anisotropy term $A_2^0\langle r^2 \rangle C_j$, thus leading to the crystal-field independent equation first proposed by Reuben in a slightly different form using Yb^{III} as a common reference[33] and recently extended by Geraldes and co-workers (eqns. 6 and 7).[32] $\langle S_z \rangle_j$ remains the only fixed parameter and

$$\frac{\Delta_{ij}}{\langle S_z \rangle_j} = \left(F_i' - F_k' \cdot \frac{G_i'}{G_k'} \right) + \frac{G_i'}{G_k'} \cdot \frac{\Delta_{kj}}{\langle S_z \rangle_j} \qquad (6)$$

$$R_{ik} = \frac{G_i'}{G_k'} = \frac{G_i}{G_k} = \frac{1 - 3\cos^2\theta_i}{1 - 3\cos^2\theta_k} \cdot \frac{r_k^3}{r_i^3} \qquad (7)$$

plots of $\Delta_{ij}/\langle S_z \rangle_j$ *vs.* $\Delta_{kj}/\langle S_z \rangle_j$ within an isostructural series are expected to be linear with a slope R_{ik} (eqn. 7) and an intercept equal to $F_i' - F_k' R_{ik}$. Since variations of the crystal-field parameter do not affect eqn. (6), any deviation from linearity leading to different slopes (R_{ik}, eqn. 7) can safely be interpreted as a geometrical change along the lanthanide series. Changes in the intercepts are more complicated to address since $F_i' - F_k' R_{ik}$ is a non-linear function which depends on geometrical changes and on possible variations of the hyperfine electron–nuclear constants.[19,32] Although combination of eqns. (4)–(6) provides an efficient tool for the reliable separation of contact and pseudo-contact contributions and subsequent accurate predictions of NMR spectra for strongly paramagnetic lanthanide-containing complexes,[23] the extraction of molecular structures in solution remains a challenge since G_i display non-linear dependencies on the axial coordinates θ_i and r_i (eqn. 3). A prior knowledge of an approximate structure is required and pure pseudo-contact contributions δ_{ij}^{pc} are then fitted by eqn. (8)

$$\delta_{ij}^{pc} = \frac{1}{12\pi r_i^3} \cdot \left[\Delta\chi_{ax}^j (3n_i^2 - 1) + \tfrac{3}{2}\Delta\chi_{rh}^j (l_i^2 - m_i^2) \right] \qquad (8)$$

to obtain axial ($\Delta\chi_{ax}$) and rhombic ($\Delta\chi_{rh}$) magnetic anisotropies together with refined polar coordinates (l_i, m_i and n_i are the direction cosines of the position vector of nucleus i with respect to the principal axis of the magnetic susceptibility tensor centred on the metal).[34]

In axial complexes for which the principal axis of the magnetic susceptibility tensor coincides with the molecular axis (at least a C_3 axis),[24] the rhombic term vanishes and Kemple *et al.*[29] propose to calculate G_i terms from the model structure according to eqn. (3) and to fit eqn. (9) to the observed

$$\Delta_{ij} = \frac{A_2^0\langle r^2 \rangle C_j}{T^2} \cdot \left(\frac{1 - 3\cos^2\theta_i}{r_i^3} \right) + \sum_i \delta_{ij}^{c} \qquad (9)$$

paramagnetic shifts Δ_{ij} by using multi-linear least-squares techniques with $A_2\langle r^2 \rangle C_j$ and contact contributions δ_{ij}^c as fitting parameters. In order to minimise the number of adjustable parameters and to obtain reliable estimations of the axial magnetic anisotropies, non-zero contact contributions (δ_{ij}^c) have been limited to nuclei separated by less than four bonds from the metallic centre.

The comparison between the magnetic parameters C_j of eqn. (3) (structure independent model)[26] and those extracted from eqn. (9) (structure dependent model) allows semi-quantitative analysis of the geometry adopted by the complex in solution. Non-linear least-squares fits of eqn. (8) or (9) have thus been attempted simultaneously to refine atomic positions[34] (or alternatively the orientation of the principal axes of the magnetic susceptibility tensor)[35] and magnetic anisotropies leading to partial determination of solution structures for macrocyclic lanthanide complexes[35] and metalloproteins.[34] Finally, the Ln–(nucleus i) distances (r_i) can independently be obtained by considering the electron-induced nuclear relaxation.[17,32,34,36] For lanthanide complexes, contact relaxation is limited to the coordinate atoms and it can be neglected for ^1H and ^{13}C NMR relaxation measurements. Both dipolar and Curie-spin terms contribute to the longitudinal (T_1) and transversal (T_2) relaxation processes according to eqns. (10) and (11) in the fast

$$\frac{1}{T_{1i}^{para}} = \frac{4}{3}\left(\frac{\mu_0}{4\pi}\right)^2 \cdot \frac{\gamma_i^2 \mu_{eff}^2}{r_i^6} \cdot \tau_e + \frac{6}{5}\left(\frac{\mu_0}{4\pi}\right)^2 \cdot \frac{\gamma_i^2 \mu_{eff}^4 H_0^2}{(3kT)^2 r_i^6} \cdot \left(\frac{\tau_r}{1 + \omega^2 \tau_r^2}\right)\left(1 - \frac{r_i^3 \delta_{ij}^{pc} N}{\bar{\chi}}\right) \qquad (10)$$

$$\frac{1}{T_{2i}^{para}} = \frac{4}{3}\left(\frac{\mu_0}{4\pi}\right)^2 \cdot \frac{\gamma_i^2 \mu_{eff}^2}{r_i^6} \cdot \tau_e + \frac{1}{5}\left(\frac{\mu_0}{4\pi}\right)^2 \cdot \frac{\gamma_i^2 \mu_{eff}^4 H_0^2}{(3kT)^2 r_i^6} \cdot \left(4\tau_r + \frac{3\tau_r}{1 + \omega^2 \tau_r^2}\right)\left(1 - \frac{r_i^3 \delta_{ij}^{pc} N}{\bar{\chi}}\right) \qquad (11)$$

motion limit.[29,30,34] τ_e and τ_r are respectively the electronic and rotational correlation times controlling dipolar and Curie-spin relaxation processes in the absence of chemical exchanges. The other terms have their usual meanings.[30,34,36] When (i) τ_r is determined by an independent experiment such as dipolar–dipole relaxation in analogous diamagnetic complexes[37] and (ii) the minor terms involving δ_{ij}^{pc} are neglected,[29] least-squares fits of $1/T_{1i}^{para}$ *vs.* $H_0^2/(1 + \omega^2\tau_r^2)$ (eqn. 10)[38] or $1/T_{2i}^{para}$ *vs.* H_0^2 (eqn. 11, $\omega^2\tau_r^2 \ll 1$)[34] allow simultaneous estimation of r_i from the slope and τ_e from the intercept. A linear combination of eqns. (10) and (11) has been proposed to remove τ_e from the fitting process thus leading to determination of r_i at a single magnetic field,[36] but this technique requires precise determination of T_{2i}^{para} which is often prevented by unresolved scalar couplings in supramolecular lanthanide complexes. When τ_r is unknown, it can be adjusted together with τ_e and r_i by using non-linear least-squares fits of eqns. (10) and (11) as similarly described for the treatment of NMRD profiles,[39] but a much simpler approach considers a nucleus sufficiently remote from the paramagnetic centre (for which the contact contribution is zero) as a reference and eqn. (10) reduces to its simplest form (eqn. 12) because the residual dipolar and Curie-spin contributions both depend on r_i^{-6}.[40,41] Relative Ln–(nucleus i) distances are thus accessible without estimations of τ_e and τ_r.

$$\frac{T_{1ref}^{para}}{T_{1i}^{para}} = \left(\frac{r_i}{r_{ref}}\right)^6 \qquad (12)$$

Results and discussion

Self-assembly of $[LnCo^{II}L_3]^{5+}$ (Ln = La to Lu or Y)

As previously reported for the self-assembly of related labile non-covalent podates $[LnML_3]^{5+}$ (M = Fe^{II}[20] or Zn^{II}[21]), the binding possibilities of the ligand strand poorly match the stereochemical preferences of M^{II} or Ln^{III} taken separately, and intricate mixtures result from titrations of L (10^{-4} M in acetonitrile) with $Co^{II}(H_2O)_6(ClO_4)_2$ or $La(ClO_4)_3 \cdot 3H_2O$. The following speciation $[LaL_3]^{3+}$, $[La_2L_3]^{6+}$, $[La_2L_2]^{6+}$ and $[La_3L_3]^{9+}$

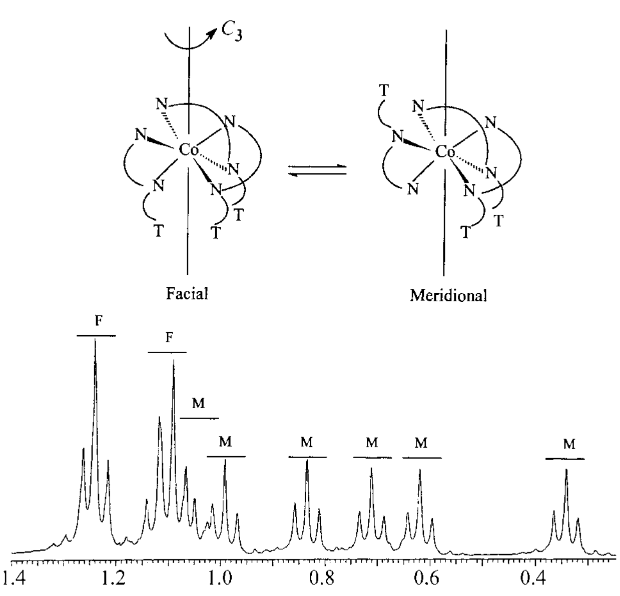

Fig. 2 Part of the ^{1}H NMR spectrum of $[CoL_3]^{2+}$ showing the signals (triplets) of Me^4 and Me^5 and their assignment to *mer*-$[CoL_3]^{2+}$ (M) and *fac*-$[CoL_3]^{2+}$ (F). T represents the tridentate binding units.

has previously been established by spectrophotometry and ^{1}H NMR.[21] Analyses of the L : Co^{II} mixtures by ESI-MS show the formation of $[CoL_3]^{2+}$, $[CoL_2]^{2+}$, $[Co_2L_3]^{4+}$ and $[Co_2L_2]^{4+}$ (ESI Table S1), but we were unable to extract reliable formation constants from spectrophotometric titrations because of the high correlation observed between the calculated UV spectra of the involved species.[42] ^{1}H NMR titrations with a larger ligand concentration (0.0245 M) confirm the existence of intricate mixtures of complexes in dynamic equilibrium on the NMR timescale except for stoichiometric Co : L ratios of 0.33 and 1.0 : 1 for which well defined inert complexes can be assigned to $[CoL_3]^{2+}$ and $[Co_2L_2]^{4+}$ in agreement with ESI-MS results. The 23 broad ^{1}H NMR singlets spread over 134 ppm ($-42 \longrightarrow 92$ ppm) observed for the latter complex are compatible with C_2 symmetrical head-to-head (HH)-$[Co_2L_2]^{4+}$ (C_2 along the Co $\cdots$ Co axis) or head-to-tail (HT)-$[Co_2L_2]^{4+}$ (C_2 perpendicular to the Co $\cdots$ Co axis) triple-stranded helicates as reported previously for (HT)-$[Zn_2L_2]^{4+}$.[21] For $[CoL_3]^{2+}$, the very complicated ^{1}H NMR spectrum ($-58 \longrightarrow 80$ ppm) corresponds to a 4 : 1 mixture (according to integration of the signals) of the C_1-symmetrical meridional (*mer*-$[CoL_3]^{2+}$) and the C_3-symmetrical facial (*fac*-$[CoL_3]^{2+}$) isomers in which Co^{II} is co-ordinated by the three bidentate binding units of the ligand strand (Fig. 2). This distribution is close the statistical ratio (3 : 1) and suggests that no major steric constraints prevent the introduction of Co^{II} into the octahedral site in heterodimetallic podates.

As previously described for (HHH)-$[LnML_3]^{5+}$ (M = Fe^{II}[20] or Zn^{II}[21]), the titration of L (10^{-4} M) with an equimolar mixture of $Co^{II}(H_2O)_6(ClO_4)_2$ and $Ln(ClO_4)_3 \cdot 3H_2O$ (Ln = La, Eu or Lu) in acetonitrile produces the expected podates (HHH)-$[LnCoL_3]^{5+}$ together with traces of $[CoL_2]^{2+}$ which are detected by ESI-MS (ESI Table S1). Concomitant spectrophotometric data obtained under the same conditions can satisfactorily be fitted[42] by eqns. (13) and (14)[20] with log

$$Ln^{3+} + Co^{2+} + 3L \rightleftharpoons [LnCoL_3]^{5+} \quad \log(\beta_{113}^{LnCo}) \qquad (13)$$

$$Co^{2+} + 2L \rightleftharpoons [CoL_2]^{2+} \quad \log(\beta_{12}^{Co}) = 14.4(6) \qquad (14)$$

$(\beta_{113}^{LaCo}) = 21.7(6)$, log $(\beta_{113}^{EuCo}) = 23.2(9)$ and log $(\beta_{113}^{LuCO}) = 23.9(6)$ which are comparable to those previously reported for (HHH)-$[LnFeL_3]^{5+}$ under the same conditions.[20]

For a total ligand concentration of 0.024 mM and a stoichiometric ratio Ln : Co : L = 1 : 1 : 3, (HHH)-$[LnCoL_3]^{5+}$ (Ln = La to Lu or Y) are the only species in solution as demonstrated by ^{1}H NMR spectra which display 23 signals typical of a head-to-head-to-head C_3-symmetrical arrangement of the strands, but spread over hundreds of ppm as a result of the fast relaxing and strongly paramagnetic Co^{II} and Ln^{III}. Reliable scalar (COSY) and dipolar (NOESY) couplings are only detected for Ln = La to Eu, Y or Lu which are either diamagnetic (Ln = La, Y or Lu) or weakly paramagnetic, thus leading to the assignments collected in Table 1. The larger magnetic moments of the remaining Ln^{III} (Ln = Tb to Er) prevent the observation of cross-peaks in 2-D NMR spectra (COSY and NOESY) and no reliable interpretation of NMR data can be obtained with classical techniques.[19] However, thorough analysis of NOE effects in (HHH)-$[LnCoL_3]^{5+}$ (Ln = La, Y or Lu) eventually demonstrates that paramagnetic Co^{II} is co-ordinated by the bidentate binding units in the pseudo-octahedral site, while the diamagnetic Ln^{III} is located in the pseudo-tricapped trigonal prismatic site produced by the remaining tridentate binding units as previously reported for (HHH)-$[LnML_3]^{5+}$ (M = Fe^{II}[20] or Zn^{II}[21]). Diffusion of diethyl ether ($C_4H_{10}O$) into concentrated solutions of (HHH)-$[LnCoL_3]^{5+}$ (Ln = La, Y or Lu) produces fair yields (73–80%) of $[LaCoL_3][ClO_4]_5 \cdot 0.25C_4H_{10}O \cdot 1.5H_2O$ **1**, $[YCoL_3][ClO_4]_5 \cdot 0.5C_4H_{10}O \cdot 2H_2O$ **2** and $[LuCoL_3][ClO_4]_5 \cdot 0.5C_4H_{10}O \cdot H_2O$ **3** as microcrystalline powders whose IR spectra are typical of $[LnML_3]^{5+}$ with ionic perchlorates and non-co-ordinating solvent molecules. Unfortunately, we were unable to obtain X-ray quality crystals for these complexes.

Post-assembly oxidation process producing (HHH)-$[LnCo^{III}L_3]^{6+}$ (Ln = La–Lu, Y)

The oxidation of labile Co^{II} (d^7 high spin) to inert Co^{III} (d^6 low spin) to give the final complexes (HHH)-$[LnCoL_3]^{6+}$ requires a clean outer sphere one-electron transfer without perturbing the co-ordination sphere. We have previously shown that the Co^{III}/Co^{II} oxidation process in the related homodimetallic triple-stranded helicate $[Co_2(L^1)_3]^{4+}$ (L^1 is the bis-bidentate ligand bis[5-(1-methyl-2-(5-methyl-2-pyridyl)benzimidazolyl)]methane) which contains two Co^{II} in pseudo-octahedral environments similar to that found in (HHH)-$[LnCoL_3]^{5+}$) occurred at 0.37 V *vs.* SCE (acetonitrile + 0.1 M NBu_4PF_6).[44] Cyclic voltammograms of (HHH)-$[LnCoL_3]^{5+}$ under the same conditions (Ln = La, Eu or Lu) display similar oxidation processes characterised by a single quasi-reversible wave at 0.41–0.43 V *vs.* SCE corresponding to Co^{III}/Co^{II} which is anodically shifted by *ca.* 0.1 V with respect to $[Co(2,2'\text{-bipy})_3]^{2+}$ (0.32 V).[43] According to a simple electrostatic model[45] considering the two metallic centres in (HHH)-$[LnCoL_3]^{5+}$ as charged dots separated by $R_{La\text{-}Co} = 8.865$ Å (taken from the crystal structure of **6**,[22] see below), the excess electrostatic work W_1 required for extracting one electron from Co^{2+} in the presence of La^{3+} is given by eqn. (15) while the related work W_2 in $[Co_2(L^1)_3]^{4+}$

$$W_1 = 3q^2/4\pi\varepsilon_0\varepsilon_r R_{La\text{-}Co} \qquad (15)$$

corresponds to eqn. (16) ($R_{Co\text{-}Co} = 8.854$ Å)[44] in which q stands

$$W_2 = 2q^2/4\pi\varepsilon_0\varepsilon_r R_{Co\text{-}Co} \qquad (16)$$

for the electrostatic charge (1.602×10^{-19} C), ε_0 the vacuum permittivity constant (8.8419×10^{-12} C^2 N^{-1} m^{-2}) and ε_r the relative dielectric constant of the medium separating the point charges and fixed at $\varepsilon_r \approx 30$ consistent with closely related triple-stranded iron(II) helicates in the same solvent and possessing similar ligand strands and intermetallic separations.[45]

The difference expressed in electrochemical potential $\Delta E_{1/2} = (W_1 - W_2)/q = 50$ mV is in good agreement with the experi-

Table 1 Experimental[a] and computed[b] ^1H NMR shifts (with respect to $SiMe_4$) of $[LnCoL_3]^{5+}$ in CD_3CN at 298 K

Compound	Bidentate binding units							
	Me^1	Me^2	H^1	H^2	H^3	H^4	H^5	H^6
$[LaCoL_3]^{5+}$	1.70	18.70	64.00	13.50	81.50	36.30	4.86	−26.50
$[YCoL_3]^{5+}$	2.05	18.70	64.50	13.70	82.70	37.00	4.71	−28.40
$[LoCoL_3]^{5+}$	1.45	18.43	64.00	13.49	81.66	36.48	4.69	−27.80
$[CeCoL_3]^{5+}$	1.29	18.60	64.00	13.40	82.80	36.60	4.40	−30.30
$[CeCoL_3]^{5+}$[b]	1.44	18.28	63.52	13.24	81.10	35.85	4.47	−28.52
$[PrCoL_3]^{5+}$	1.14	18.33	64.00	13.29	82.50	36.30	4.21	−31.70
$[PrCoL_3]^{5+}$[b]	1.32	18.04	63.22	13.07	80.85	35.53	4.17	−29.74
$[NdCoL_3]^{5+}$	1.38	18.54	64.00	13.38	82.24	36.50	4.52	−29.60
$[NdCoL_3]^{5+}$[b]	1.51	18.39	63.63	13.31	81.20	35.96	4.55	−27.95
$[EuCoL_3]^{5+}$	1.51	18.90	64.50	13.65	81.50	36.73	5.14	−25.00
$[EuCoL_3]^{5+}$[b]	2.26	19.03	64.85	13.94	83.03	37.39	5.06	−26.73
$[TbCoL_3]^{5+}$	−1.60	13.86	58.50	10.17	77.67	31.63	0.56	−55.00
$[TbCoL_3]^{5+}$[b]	−0.66	14.06	59.48	10.72	78.26	31.58	0.36	−50.39
$[DyCoL_3]^{5+}$	−1.04	13.83	58.35	10.18	78.36	31.65	−0.20	−57.00
$[DyCoL_3]^{5+}$[b]	−0.73	13.60	57.57	10.49	77.92	31.04	−0.88	−51.97
$[HoCoL_3]^{5+}$	0.46	16.02	61.00	11.72	80.57	34.11	2.07	−45.00
$[HoCoL_3]^{5+}$[b]	0.43	15.94	61.47	11.92	80.05	34.03	2.07	−41.39
$[ErCoL_3]^{5+}$	1.84	19.47	64.58	14.12	83.66	37.82	5.41	−25.00
$[ErCoL_3]^{5+}$[b]	1.79	19.03	64.58	13.88	82.20	37.24	5.42	−25.10
$[TmCoL_3]^{5+}$	2.67	20.65	66.60	14.95	84.47	39.08	6.34	−17.62
$[TmCoL_3]^{5+}$[b]	2.42	20.13	65.79	14.57	83.25	38.64	6.75	−20.00
$[YbCoL_3]^{5+}$	1.87	19.41	65.00	14.13	83.42	37.75	5.44	−24.40
$[YbCoL_3]^{5+}$[b]	1.86	19.11	64.70	13.93	82.29	37.34	5.53	−24.64

Compound	Tridentate binding units								
	H^9	H^{10}	H^{11}	H^{12}	H^{13}	H^{14}	Me^3	Me^4	Me^5
$[LaCoL_3]^{5+}$	−8.27	6.25	5.78	5.89	6.62	5.90	2.29	−0.85	−0.40
$[YCoL_3]^{5+}$	−8.99	5.90	5.34	5.79	6.50	5.82	2.05	−0.39	−1.03
$]LuCoL_3]^{5+}$	−9.00	5.90	5.31	5.83	6.50	5.85	2.05	−1.02	−0.35
$[CeCoL_3]^{5+}$	−14.90	5.65	5.80	8.36	8.43	7.10	3.20	−0.10	−3.00
$[CeCoL_3]^{5+}$[b]	−14.55	5.77	5.97	8.30	8.28	7.02	3.23	0.09	−2.93
$[PrCoL_3]^{5+}$	−18.60	5.35	6.12	10.43	9.46	8.09	3.88	0.40	−4.60
$[PrCoL_3]^{5+}$[b]	−18.55	5.51	6.35	10.14	9.26	7.93	3.93	0.59	−4.43
$[NdCoL_3]^{5+}$	−12.90	5.73	6.26	8.66	8.19	7.47	2.89	0.03	−2.60
$[NdCoL_3]^{5+}$[b]	−12.57	5.89	6.47	8.49	8.08	7.39	2.95	0.23	−2.53
$[EuCoL_3]^{5+}$	−4.05	6.49	4.24	1.85	4.56	3.46	2.13	−1.00	1.05
$[EuCoL_3]^{5+}$[b]	−4.49	6.30	4.02	1.93	4.63	3.49	1.44	−1.29	1.06
$[TbCoL_3]^{5+}$	−85.50	0.89	2.03	29.75	21.66	16.10	16.07	3.85	−30.04
$[TbCoL_3]^{5+}$[b]	−82.41	0.75	2.63	25.41	19.26	13.99	14.67	2.99	−25.44
$[DyCoL_3]^{5+}$	−95.00	0.65	2.90	32.40	22.80	17.20	17.53	5.85	−34.00
$[DyCoL_3]^{5+}$[b]	−90.41	0.35	3.78	28.36	20.91	15.99	16.40	5.40	−30.10
$[HoCoL_3]^{5+}$	−54.50	2.80	3.43	15.75	12.95	8.10	11.08	3.06	−19.85
$[HoCoL_3]^{5+}$[b]	−51.81	3.05	3.89	17.76	14.21	11.79	10.10	0.86	−16.40
$[ErCoL_3]^{5+}$	0.32	6.68	3.86	−3.51	−0.10	0.70	0.97	−1.16	2.65
$[ErCoL_3]^{5+}$[b]	−1.31	6.45	3.78	0.10	2.79	2.36	1.01	−0.68	1.71
$[TmCoL_3]^{5+}$	19.80	7.76	4.41	−8.91	−6.28	−1.86	−2.74	−2.74	10.54
$[TmCoL_3]^{5+}$[b]	15.69	7.21	4.18	−3.76	−0.54	0.79	−1.59	−2.11	7.12
$[YbCoL_3]^{5+}$	3.35	6.52	4.98	−0.34	1.55	3.67	0.08	−1.58	3.91
$[YbCoL_3]^{5+}$[b]	1.09	6.40	4.90	2.32	4.41	4.27	0.46	−1.11	2.37

[a] Sm^{III} is not considered because of its weak paramagnetism. [b] Chemical shift calculated with eqn. (20) (see text).

mental difference of 60 mV observed between the oxidation potentials of (HHH)-$[LaCoL_3]^{5+}$ and $[Co_2(L^1)_3]^{4+}$ (Table 2). We conclude that (i) the lanthanide(III) site does not induce major steric constraints on the Co^{II} and (ii) compared with $[Co_2(L^1)_3]^{4+}$, the $Co^{II/III}$ oxidation in (HHH)-$[LnCoL_3]^{5+}$ is only delayed by the higher charge of the neighbouring lanthanide cation. According to our results, bromine ($E_{1/2} = 0.99$ V *vs.* SCE; CH_3CN + 0.1 M NBu_4PF_6) is thus a suitable outer sphere oxidant for (HHH)-$[LnCo^{II}L_3]^{5+}$ (Ln = La to Lu) and we expect quantitative transformations into the inert podates (HHH)-$[LnCo^{III}L_3]^{6+}$. This process can easily be followed by ^1H NMR since paramagnetic high spin Co^{II} is transformed into diamagnetic low spin Co^{III} (Fig. 3). Detailed analysis of the NMR spectra of (HHH)-$[LnCo^{III}L_3]^{6+}$ (Ln = La to Lu except for Pm)[19,23] shows exclusive formation of the expected head-to-head-to-head C_3-symmetrical non-covalent podate in which Co^{III} occupies the pseudo-octahedral site produced by the three wrapped bidentate binding units, and Ln^{III} lies in the remaining nine co-ordinate N_6O_3 pseudo-tricapped trigonal prismatic site. Slow diffusion of diethyl ether gives $[LaCoL_3][ClO_4]_5Br{\cdot}0.5H_2O$ **4** (yield = 95%) whose bromide counter anion can be exchanged by metathesis with $AgClO_4$ in acetonitrile to give $[LaCoL_3][ClO_4]_6{\cdot}0.1C_4H_{10}O{\cdot}2.4H_2O$ **5** after filtration of AgBr and crystallisation from acetonitrile–diethyl ether. Slow diffusion of diisopropyl ether into a concentrated solution of **5** provides X-ray quality prisms of $[LaCoL_3][ClO_4]_{5.5}(OH)_{0.5}{\cdot}4CH_3CN{\cdot}2H_2O$ **6**[22] but a similar procedure with Ln = Lu failed. Fragile yellow X-ray quality prisms of $[LuCoL_3][CF_3SO_3]_6{\cdot}2CH_3CN{\cdot}H_2O$ **7** are obtained when 30 equivalents of $NBu_4CF_3SO_3$ are added to the mother liquor prior to diffusion of diisopropyl ether.

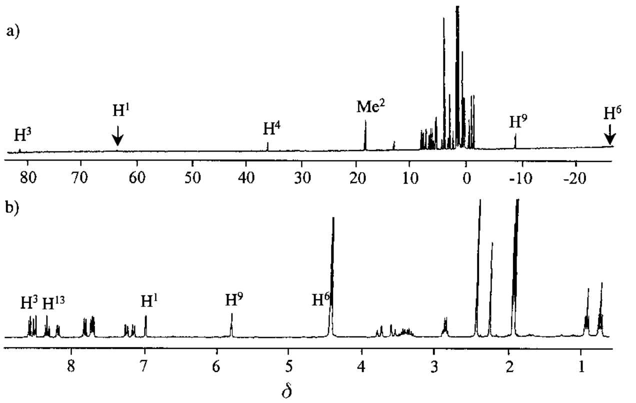

Fig. 3 ^{1}H NMR spectra in CD_3CN of (a) (HHH)-$[LaCo^{II}L_3]^{5+}$ and (b) (HHH)-$[LaCo^{III}L_3]^{6+}$ (adapted from ref. 22).

Table 2 Electrochemical reduction potentials in CH_3CN + 0.1 M NBu_4PF_6^{a} at 293 K

Compound	$E_{1/2}$	$E_p^a - E_p^c$	Attribution	Ref.
$[LaCoL_3]^{5+}$	+0.43	100	Co^{III}/Co^{II}	This work
	−1.16	115	Co^{II}/Co^{I}	
$[EuCoL_3]^{5+}$	+0.42	130	Co^{III}/Co^{II}	This work
	−0.56	120	Eu^{III}/Eu^{II}	
	−1.20	95	Co^{II}/Co^{I}	
$[LuCoL_3]^{5+}$	+0.41	150	Co^{III}/Co^{II}	This work
	−1.12	115	Co^{II}/Co^{I}	
$[CoL_3]^{2+}$	+0.44	80	Co^{III}/Co^{II}	This work
	−1.15	75	Co^{II}/Co^{I}	
$[Co_2(L^1)_3]^{4+}$	+0.37	160	Co^{III}/Co^{II}	44
	−1.19	90	Co^{II}/Co^{I}	

^{a} Potentials given in V *vs.* SCE and ($E_p^a - E_p^c$) in mV; estimated error in $E_{1/2}$ is ± 0.01 V.

Crystal and molecular structure of $[LuCoL_3][CF_3SO_3]_6\cdot 2CH_3CN\cdot H_2O$ 7

In order to investigate possible geometrical variations along the lanthanide series and to obtain valuable models for solution structures, the crystal structures of non-covalent podates (HHH)-$[LnCo^{III}L_3](anion)_6$ have been solved for the largest (Ln = La; nine-co-ordinate ionic radius $R^{La}_{CN=9} = 1.216$ Å;[46] **6**) and the smallest (Ln = Lu; nine-co-ordinate ionic radius $R^{Lu}_{CN=9} = 1.032$ Å;[46] **7**) lanthanides. The crystal and molecular structure of **6** has previously been described in a preliminary communication.[22] As found for **6**, the crystal structure of **7** consists of discrete (HHH)-$[LuCo^{III}L_3]^{6+}$ cations, unco-ordinated and disordered anions and solvent molecules. One of the ethyl groups (C29a, C30a) displays a cross disorder which has been refined with four atomic sites (see Experimental section and Fig. 4), but only the major conformer (PP = 0.6) is shown in Fig. 5. Fig. 4 shows the atomic numbering scheme, Fig. 5 displays ORTEP[47] views of (HHH)-$[LaCo^{III}L_3]^{6+}$ **6**[22] and (HHH)-$[LuCo^{III}L_3]^{6+}$ **7** in similar orientations and Table 3 collects selected bond distances and angles for **7**.

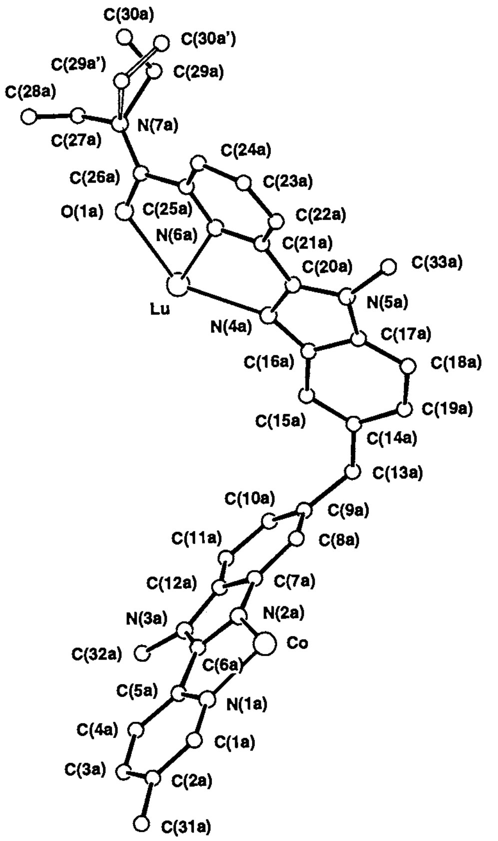

Fig. 4 Numbering scheme for the cation (HHH)-$[LuCo^{III}L_3]^{6+}$ in complex **7**. Indexes b and c correspond to the other strands.

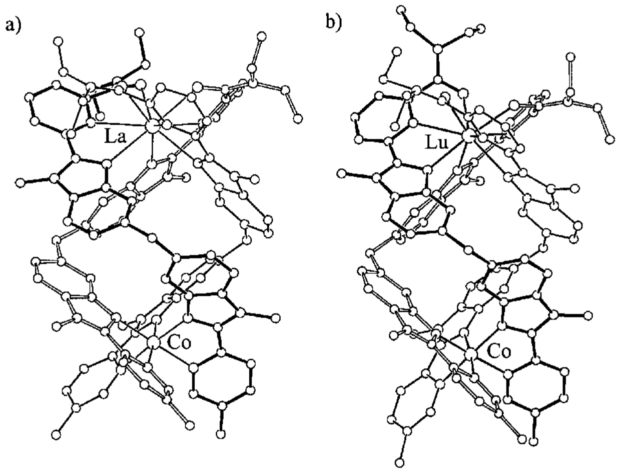

Fig. 5 ORTEP[47] views of (a) (HHH)-$[LaCo^{III}L_3]^{6+}$ and (b) (HHH)-$[LuCo^{III}L_3]^{6+}$ perpendicular to the pseudo-C_3 axis (adapted from ref. 19).

The molecular structure of (HHH)-$[LuCo^{III}L_3]^{6+}$ confirms the formation of the pseudo-C_3 symmetrical head-to-head-to-head triple-helical cation in the solid state. The helical twist of the strands results from successive rotations about the C–C bonds connecting the aromatic rings with maximum values between the benzimidazole rings connected by the methylene spacers (average interplanar angle = 87.4°) which is similar to that found for (HHH)-$[LaCo^{III}L_3]^{6+}$ (85.2°).[22] Although a larger Ln···Co contact distance is observed in (HHH)-$[LuCo^{III}L_3]^{6+}$ (9.234(2) compared to 8.865(4) Å for **6**), the interplanar angles are similar for both structures (ESI Table S2). In order to address this problem, we have considered the triple helices as being constituted of four helical portions packed along the pseudo-C_3 axis and delimited by five facial planes F_1–F_5 (F_1: N1a, N1b, N1c. F_2: N2a, N2b, N2c. F_3: N4a, N4b, N4c. F_4: N6a, N6b, N6c. F_5: O1a, O1b, O1c) which are almost parallel (interplanar angles 1–18° for $[LuCo^{III}L_3]^{6+}$ and 1–4° for $[LaCo^{III}L_3]^{6+}$ ESI Tables S2 and S3). Each helical portion F_1–F_2, F_2–F_3, F_3–F_4 and F_4–F_5 is then characterised by its pitch (P_{ij})[48] estimated by $P_{ij} = d(F_i–F_j)/(a_{ij}/360)$.[49] $d(F_i–F_j)$ is the distance between the facial planes *i* and *j* and a_{ij} the average twist angle (in degrees) between the projections of N*i* and N*j* (or O*j*) belonging to the same ligand strand onto an intermediate plane passing through the metal (Fig. 6 and Table 4).[50] P_{ij} strongly vary along the helical axis pointing to a tightened helical twist around the co-ordinated metal ions (portions F_1–F_2, F_3–F_4 and F_4–F_5) and a relaxed wrapping in the intermetallic portion (F_2–F_3). These variations are more pronounced in complex **7**,

Table 3 Selected bond distances (Å) and angle (°) for $[LuCoL_3][CF_3SO_3]_6 \cdot 2CH_3CN \cdot H_2O$ **7**

	ligand a	ligand b	ligand c
Lu···Co	9.234(2)		
Lu–O(1)	2.316(5)	2.339(5)	2.340(5)
Lu–N(4)	2.474(5)	2.495(6)	2.516(6)
Lu–N(6)	2.526(6)	2.518(6)	2.508(6)
Co–N(1)	1.955(6)	1.962(6)	1.956(6)
Co–N(2)	1.929(6)	1.914(6)	1.925(6)
	Bite angles		
	ligand a	ligand b	ligand c
N(1)–Co–N(2)	83.2(2)	82.1(2)	83.1(2)
N(4)–Lu–N(6)	65.1(2)	64.0(2)	64.6(2)
N(6)–Lu–O(1)	63.3(2)	64.1(2)	65.9(2)
N(4)–Lu–O(1)	128.3(2)	128.0(2)	130.2(2)
N–Co–N			
N(1a)–Co–N(2b)	88.2(2)	N(1a)–Co–N(1c)	94.8(2)
N(1a)–Co–N(2c)	176.2(2)	N(2a)–Co–N(1b)	178.6(2)
N(2a)–Co–N(2b)	97.6(2)	N(2a)–Co–N(1c)	86.5(2)
N(2a)–Co–N(2c)	93.6(2)	N(1a)–Co–N(1b)	95.4(2)
N(1b)–Co–N(1c)	93.9(2)	N(1b)–Co–N(2c)	87.8(2)
N(2b)–Co–N(1c)	175.2(2)	N(2b)–Co–N(2c)	94.1(2)
N–Lu–N			
N(4a)–Lu–N(4b)	86.9(2)	N(6a)–Lu–N(6b)	119.7(2)
N(4b)–Lu–N(4c)	86.2(2)	N(6b)–Lu–N(6c)	124.0(2)
N(4a)–Lu–N(4c)	80.5(2)	N(6a)–Lu–N(6c)	114.8(2)
N(4a)–Lu–N(6c)	142.2(2)	N(4a)–Lu–N(6b)	76.1(2)
N(6a)–Lu–N(4b)	147.6(2)	N(4b)–Lu–N(6c)	77.2(2)
N(6b)–Lu–N(4c)	142.6(2)	N(6a)–Lu–N(4c)	74.0(2)
O–Lu–N			
N(4a)–Lu–O(1c)	143.8(2)	N(4a)–Lu–O(1b)	82.8(2)
N(6a)–Lu–O(1b)	66.7(2)	N(6a)–Lu–O(1c)	134.1(2)
N(6b)–Lu–O(1c)	67.7(2)	N(4b)–Lu–O(1c)	78.1(2)
O(1a)–Lu–N(6b)	131.8(2)	O(1a)–Lu–N(4b)	141.6(2)
O(1a)–Lu–N(4c)	85.5(2)	O(1a)–Lu–N(6c)	65.4(2)
O(1b)–Lu–N(4c)	140.7(2)	O(1b)–Lu–N(6c)	133.7(2)
O–Lu–O			
O(1a)–Lu–O(1b)	77.5(2)	O(1b)–Lu–O(1c)	81.1(2)
O(1a)–Lu–O(1c)	78.9(2)		

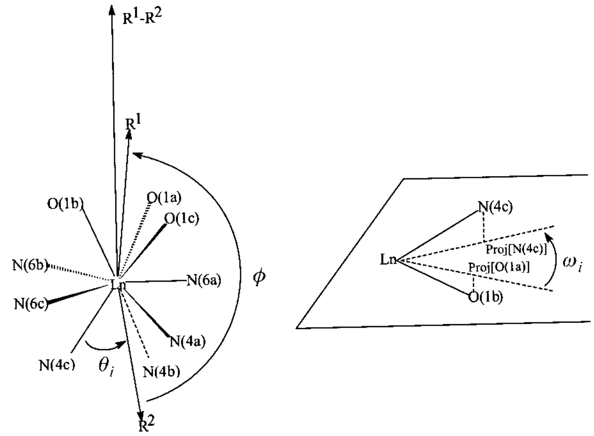

Fig. 6 Definition of ϕ, θ_i and ω_i for a pseudo-tricapped trigonal prismatic site (R^2 = Ln–N4a + Ln–N4b + Ln–N4c and R^1 = Ln–O1a + Ln–O1b + Ln–O1c).[50] Proj[N(i)] is the projection of N(i) along the R^1–R^2 direction onto a perpendicular plane passing through the metal.[50] The same analysis holds for the pseudo-octahedral sites when Ln^{III} is replaced by Co^{III}, O1i and N4i by N1i and N2i respectively and N6i are omitted (R^1 = Co–N1a + Co–N1b + Co–N1c and R^2 = Co–N2a + Co–N2b + Co–N2c).[44]

Table 4 Helical pitches P_{ij} and linear distances (both in Å) along the pseudo-C_3 axis in $[LaCoL_3][ClO_4]_{5.5}[OH]_{0.5} \cdot 4CH_3CN \cdot 2H_2O$ **6** and $[LuCoL_3][CF_3SO_3] \cdot 2CH_3CN \cdot H_2O$ **7**

	$[LaCo^{III}L_3]^{6+}$	$[LuCo^{III}L_3]^{6+}$
Ln···Co	8.8648	9.234
F_1–Co[a]	1.047	1.034
Co–F_2	0.989	1.006
F_2–F_3	6.328	6.658
F_3–Ln	1.548	1.570
Ln–F_5	1.629	1.578
P_{12}	13.20	13.05
P_{23}	19.74	20.42
P_{34}	11.04	10.84
P_{45}	10.83	9.72
P_{15}	13.70	13.51

[a] F_1: N1a, N1b, N1c. F_2: N2a, N2b, N2c. F_3: N4a, N4b, N4c. F_4: N6a, N6b, N6c. F_5: O1a, O1b, O1c.

but the average helical pitches are comparable for $[LuCo^{III}L_3]^{6+}$ (P_{15} = 13.5 Å) and $[LaCo^{III}L_3]^{6+}$ (P_{15} = 13.7 Å). However, the F_2–F_3 helical domain corresponds to the larger portion of the helix (55%) and its larger pitch in **7** (*i.e.* its reduced helical twist) is responsible for the increased intermetallic Lu···Co distances. Moreover, the less tightened wrapping of the latter domain in $[LuCo^{III}L_3]^{6+}$ is confirmed by the smaller triangular surface defined by the carbon atoms of the methylene spacers C13a C13b, C13c which amounts to 24.7 Å^2 for **7** and 26.9 Å^2 for **6**.

A detailed geometrical analysis of the nine-co-ordinate pseudo-tricapped trigonal prismatic lanthanide sites based on the determination of the angles ϕ, θ_i and ω_i (Fig. 6)[50] as described previously for $[LnFeL_3]^{5+}$[20] (ESI Table S4) shows only faint differences between $[LaCo^{III}L_3]^{6+}$ and $[LuCo^{III}L_3]^{6+}$. The main discrepancies concern the expected contraction of the ligand–metal bond distances.[46] In $[LaCo^{III}L_3]^{6+}$ the La–N(bzim) (2.61(2)–2.79(2), average 2.67(3) Å) are slightly shorter than La–N(py) (2.72(2)–2.78(2), average 2.74(3) Å) as similarly found for $[LuCo^{III}L_3]^{6+}$ (Lu–N(bzim) (2.474(5)–2.516(6), average 2.50(1) Å) and Lu–N(py) (2.508(6)–2.526(6), average 2.52(1)Å), but the Lu–O(amide) bond distances strongly deviate (2.136(5)–2.340(5) Å) from the average value (2.27(4) Å) due to a closer approach of the terminal carboxamide group of ligand a. No related distortion was observed for the La–O(amide) bonds (2.48(2)–2.53(2), average 2.50(2) Å) and calculations of the ionic radii according to Shannon's definition with r(N) = 1.46 Å and r(O) = 1.31 Å give R^{La} = 1.23 Å and R^{Lu} = 1.018 Å in qualitative good agreement with statistical values for nine-co-ordinate La^{III} and Lu^{III}.[46] Finally, Lu^{III} lies out of the facial plane F_4 defined by the pyridine nitrogen atoms N6i (0.179 Å toward Co^{III}) in **7** while La^{III} exhibits a related smaller shift (0.104 Å).

The co-ordination spheres of Co^{III} in $[LnCo^{III}L_3]^{6+}$ (Ln = La or Lu) are best described as distorted octahedra flattened along the molecular pseudo-C_3 axis. Again the detailed geometrical analysis according to Fig. 6[44] shows only small variations between complexes **6** and **7** (ESI Table S5). The Co–N bond distances are standard[51] in $[LuCo^{III}L_3]^{6+}$ (average Co–N(py) = 1.958(6), average Co–N(bzim) = 1.923(8) Å) and can be compared to 1.96(3) and 1.92(3) Å found in the triple-stranded helicate $[Co_2(L^1)_3]^{6+}$.[52] These distances are slightly longer in $[LaCo^{III}L_3]^{6+}$ (2.03(2) and 1.96(3) Å)[22] which strongly suggests that the Co–N bonds are stretched to accommodate the large La^{III} in the second co-ordination site. We thus conclude that replacement of La^{III} by Lu^{III} in (HHH)-$[LnCo^{III}L_3]^{6+}$ (Ln = La or Lu) has only minor effects on the triple-helical structures of the cations in the solid state except for (i) the expected 7–10% contraction of the Ln–N and Ln–O bonds when going from La to Lu and (iii) a slight tightening of the Co–N bonds resulting from mechanical couplings between the metallic sites. The triple-helical cations (HHH)-$[LuCo^{III}L_3]^{6+}$

are packed in the crystal with their pseudo-C_3 axis roughly aligned with the b direction thus forming columns in a pseudo-hexagonal arrangement. The triflate anions and solvent molecules occupy the interstices between the columns (ESI Fig. S1).

Solution structure of (HHH)-$[LnCo^{III}L_3]^{6+}$ by paramagnetic NMR

The complete series of non-covalent podates (HHH)-$[LnCo^{III}L_3]^{6+}$ (Ln = La to Lu or Y except Pm) has been prepared *in situ* by quantitative bromine oxidation of (HHH)-$[LnCo^{II}L_3]^{5+}$ for NMR investigations. Classical scalar and dipolar couplings in two-dimensional COSY and NOESY spectra allow the reliable assignment of H^{1-6}, H^{9-14} and Me^{1-5} reported in ESI Table S6[19] for diamagnetic (Ln = La, Y or Lu) or weakly paramagnetic (Ln = Ce to Eu, Tm or Yb) complexes, but the diastereotopic pairs $H^{7,8}$, $H^{15,16}$ and $H^{17,18}$ are excluded since unambiguous assignments of AB spin systems are not available. Treatment of these data according to the structure independent, but crystal-field dependent Reilley method (eqns. 4 and 5) shows systematic breaks and gives straight lines for Ln = Ce to Eu which do not contain Tm and Yb.[19] Iterative calculations using this preliminary set of F_i' and $G_i'A_2^0\langle r^2\rangle$ allow satisfying predictions for the ^1H NMR spectra of (HHH)-$[LnCo^{III}L_3]^{6+}$ (Ln = Tb or Dy) only, but Ln = Er or Ho escape identification.[19,23] Removal of the crystal-field and axial magnetic anisotropy parameters in eqn. (6) provides straight lines for the complete lanthanide series Ce to Yb pointing to a single structure for all complexes in solution. The use of free ion $\langle S_z\rangle_j$ terms for Ln = Er or Ho[25] and the paramagnetic shift of one particular proton taken as a reference in (HHH)-$[LnCo^{III}L_3]^{6+}$ provide successful predictions of ^1H NMR spectra and subsequent assignments which eventually establish the existence of two straight lines according to Reilley's method corresponding to Ln = Ce to Eu and Tb to Yb.[23] F_i' and $G_i'A_2^0\langle r^2\rangle$ terms for the two series are collected in Table 5.[23] Recent studies of magnetic anisotropies in paramagnetic macromolecules demonstrate that the theoretical Bleaney coefficients (C_j) are corroborated by experimental determinations[34,53] and we can thus safely assign the breaks according to eqns. (4) and (5) to a concomitant change of $A_2^0\langle r^2\rangle$ and F_i' occurring when the 4f shell is more than half-filled.[23] $G_i'A_2^0\langle r^2\rangle$ terms found for the two series Ln = Ce to Eu and Tb to Yb systematically differ by a constant ratio which is assigned to a change of the crystal-field parameter within the isostructural series ($A_2^0\langle r^2\rangle_{Ln=Ce-Eu}/A_2^0\langle r^2\rangle_{Ln=Tb-Yb} = 1.6(2)$). This points to larger ligand–Ln^{III} interactions in the first series consistent with the spatial diffuseness of 4f electronic orbitals.[23]

Although the combination of structure independent techniques (eqns. 4–6) is an efficient tool for investigating isostructurality and spin delocalisation in paramagnetic lanthanide complexes, no information is obtained concerning the 3-D geometrical structure of these complexes in solution except for (i) the C_3 symmetry on the NMR timescale (magnetic equivalence of the three strands, diastereotopic protons $H^{7,8}$ and interstrand NOE effects)[19–23] and (ii) the co-ordination of Ln^{III} to the tridentate binding unit. Extraction of the molecular structure in solution with a minimum of adjustable parameters is thus a crucial point to test the validity of the paramagnetic NMR techniques and their reliability to analyse solution structures. Since G_i depends non-linearly on the axial coordinates θ_i and r_i (eqn. 3), no direct access to the molecular geometry can be obtained from pseudo-contact contributions (δ_{ij}^{pc}) without resorting to a structural model unless θ_i and/or r_i can be obtained by an independent technique. According to eqn. (10), the field dependence of relaxation processes through the Curie-spin contribution might give r_i values through *linear* least-squares fits of $1/T_{1i}^{para}$ *vs.* $H_0^2/(1 + \omega^2\tau_r^2)$ providing that the rotational correlation time τ_r is determined by an independent method.[29,34,36] Attempts to use the ^{13}C–^1H intermolecular dipolar–dipole relaxation processes in diamagnetic complexes (HHH)-$[LnCo^{III}L_3]^{6+}$ (Ln = La or Lu) provide anomalously short and dispersed $\tau_r = 67(20)$ and 23(8) ps respectively which can be compared to $\tau_r = 61$–68 ps for $[Ln(OH_2)_{8-9}]^{3+}$,[54] 41(2) ps for $[Gd(OH_2)_8]^{3+}$[55] and 80 ps for $[Lu(DOTA)]^-$[36] in water, and $\tau_r = 51$ ps for $[Ln(CH_3CN)_{8-9}]^{3+}$ in acetonitrile.[56] Some peculiar hydrophobic effects have been invoked to rationalise unusually short τ_r for spherical trimetallic complexes in water,[39] but attempts to fit paramagnetic longitudinal relaxation rates according to eqn. (10) with $\tau_r = 67$ ps give only inappropriate values of r_i and τ_e ($1/T_{1i}^{para} = (1/T_{1i}^{exp}) - (1/T_{1i}^{dia})$ at 200, 300, 400, 500 and 600 MHz; ESI Table S7).‡ As we seriously doubt from the rotational time τ_r found by the method of Wasylishen,[37] we have resorted to eqn. (12) to extract reasonable r_i distances for the strongly paramagnetic complexes (HHH)-$[LnCo^{III}L_3]^{6+}$ (Ln = Tb or Tm) when $r_{H^4} = 8.18$ Å (from the crystal structure of **7**) is used as a reference. The calculated distances (Table 6) are in qualitative agreement with those found in the crystal structures of (HHH)-$[LnCo^{III}L_3]^{6+}$ (Ln = La, **6**; Lu, **7**) and demonstrate that the molecular solid state structures are close to the solution structures. More realistic τ_r values can be obtained by introducing into eqn. (10) the r_i distances taken from the crystal structure of **7** and $\tau_e = 0.2$ ps[57] for (HHH)-$[TbCo^{III}L_3]^{6+}$. We obtain for all studied protons an average value of $\tau_r = 200(15)$ ps compatible with the cylindrical shape and molecular weight of the cation which can be compared with that of gadolinium(III) calix[4]arene complex under the same conditions ($\tau_r = 193$ ps, acetonitrile, 298 K).[56] The field dependence of $1/T_{1i}^{para}$ can be then used to obtain the set of r_i and τ_e values collected in Table 6 which strongly supports similar structures in the solid state and in solution (ESI Fig. S2). As the field dependence of the Curie-spin contribution to $1/T_{1i}^{para}$ may suffer from $\omega^2\tau_r^2$ dispersion effects[54] which are removed for transversal relaxation ($1/T_{2i}^{para}$, eqn. 11), we have confirmed that similar r_i and τ_e values are obtained for H^{11-14} in (HHH)-$[TbCo^{III}L_3]^{6+}$ (ESI Tables S8, S9 and Fig. S3) when T_2^{para} is roughly estimated as the half-width at half-height of the NMR signal (neglect of scalar coupling, field inhomogeneity and diamagnetic contributions).‡ We conclude from the relaxation measurements that (i) the estimated rotational correlation time $\tau_r = 200(15)$ ps is acceptable and long enough to obtain reliable field dependence of the Curie-spin effect for both T_1^{para} and T_2^{para} thus allowing the determination of r_i, (ii) the dipolar C–H coupling fails to give interpretable values for τ_r in our hands and (iii) the Ln–H^i distances are similar in the crystal structures of (HHH)-$[LnCo^{III}L_3]^{6+}$ (Ln = La or Lu) and in the solution structures of (HHH)-$[LnCo^{III}L_3]^{6+}$ (Ln = Tb or Tm).

A qualitative and quantitative comparison of solid state and solution structures can finally be addressed by calculating G_i factors from the C_3-average crystal structures of the cations (HHH)-$[LnCo^{III}L_3]^{6+}$ in complexes **6** and **7** and fitting the experimental paramagnetic shifts Δ_{ij} by eqn. (9) with multilinear least-squares techniques.[29] Both techniques for averaging G_i values over the three strands have been checked (averaging θ_i and r_i for the three strands and then calculating G_i or calculating G_i for each proton and then averaging G_i for symmetry related protons)[19] and give no significant differences. Contact contributions δ_{ij}^c are limited to protons remote from Ln^{III} by less than five bonds, leading to only five significant contributions for H^9 and H^{11-14} in agreement with contact terms obtained with the structure independent Reilley method $|F_i'| \geq 0.07$ (Table 5). Fitting by eqn. (9) for each Ln^{III} (except Sm^{III} because

---

‡ A strict dependence of $1/T_{1i}^{para}$ *vs.* H_0^2 or $1/T_{2i}^{para}$ *vs.* H_0^2 is only observed when $\omega^2\tau_r^2 \ll 1$ because ω depends on H_0. This simplification is justified for several protons in (HHH)-$[TbCo^{III}L_3]^{6+}$, but we have systematically plotted $1/T_{1i}^{para}$ *vs.* $H_0^2/(1 + \omega^2\tau_r^2)$ to obtain the r_i and τ_e values collected in Table 6 (ESI Fig. S2). For the approximate T_{2i}^{para} values, plots of $1/T_{2i}^{para}$ *vs.* H_0^2 are satisfactory (ESI Fig. S3).

Table 5 Hyperfine coupling constants F'_i and structural parameters $G'_iA_2^0\langle r^2\rangle$ for aromatic and methyl protons in complexes (HHH)-$[LnCo^{III}L_3]^{6+}$ and (HHH)-$[LnCo^{II}L_3]^{5+}$ (Ln = Ce to Eu and Tb to Yb) in CD_3CN (298 K)

			Bidentate binding unit								
Compound		Method[a]	Me^1	Me^2	H^1	H^2	H^3	H^4	H^5	H^6	Ref.
$[LnCo^{III}L_3]^{6+}$	F'_i	eqns. (4), (5)[30]	−0.01(1)	−0.01(1)	−0.01(1)	−0.01(1)	−0.01(1)	−0.01(1)	−0.01(1)	−0.05(1)	23
Ln = Ce to Eu	$G'_iA_2^0\langle r^2\rangle$	eqns. (4), (5)[30]	0.035(3)	0.060(3)	0.071(3)	0.038(1)	0.058(2)	0.068(1)	0.060(1)	0.29(1)	23
$[LnCo^{III}L_3]^{6+}$	F'_i	eqns. (4), (5)[30]	0.03(1)	0.05(1)	0.06(1)	0.03(1)	0.05(1)	0.05(1)	0.04(1)	0.22(2)	23
Ln = Tb to Yb	$G'_iA_2^0\langle r^2\rangle$	eqns. (4), (5)[30]	0.021(1)	0.38(1)	0.045(5)	0.024(1)	0.036(1)	0.046(1)	0.043(3)	0.177(1)	23
$[LnCo^{III}L_3]^{6+}$	F'_i	eqn. (9)[29]	—	—	0(0)	0(0)	0(0)	0(0)	0(0)	0(0)	This work
Ln = Ce to Eu	$G'_iA_2^0\langle r^2\rangle$	eqn. (9)[29]	—	—	0.082(2)	0.050(1)	0.074(2)	0.085(2)	0.069(2)	0.345(7)	This work
$[LnCo^{III}L_3]^{6+}$	F'_i	eqn. (9)[29]	—	—	0(0)	0(0)	0(0)	0(0)	0(0)	0(0)	This work
Ln = Tb to Yb	$G'_iA_2^0\langle r^2\rangle$	eqn. (9)[29]	—	—	0.048(1)	0.029(1)	0.043(1)	0.050(1)	0.039(1)	0.201(5)	This work
$[Ln\ Co^{II}L_3]^{5+}$	F'_i	eqns. (4), (5)[30]	0.07(2)	−0.01(1)	0(0)	0.01(1)	0.07(5)	0.02(2)	−0.02(2)	0.15(7)	This work
Ln = Ce to Eu	$G'_iA_2^0\langle r^2\rangle$	eqns. (4), (5)[30]	0.08(2)	0.027(6)	0(0)	0.022(5)	−0.10(4)	0.01(2)	0.058(6)	0.48(6)	This work
$[LnCo^{II}L_3]^{5+}$	F'_i	eqns. (4), (5)[30]	0.03(1)	0.03(1)	0.05(1)	0.026(5)	−0.01(2)	0.02(1)	0.04(1)	0.30(5)	This work
Ln = Tb to Yb	$G'_iA_2^0\langle r^2\rangle$	eqns. (4), (5)[30]	0.026(3)	0.044(2)	0.050(3)	0.030(2)	0.053(6)	0.051(3)	0.037(2)	0.20(2)	This work
$[LnCo^{II}L_3]^{5+}$	F'_i	eqn. (9)[29]	—	—	0(0)	0(0)	0(0)	0(0)	0(0)	0(0)	This work
Ln = Ce to Eu	$G'_iA_2^0\langle r^2\rangle$	eqn. (9)[29]	—	—	0.12(3)	0.08(2)	0.11(3)	0.19(3)	0.10(3)	0.5(1)	This work
$[LnCo^{II}L_3]^{5+}$	F'_i	eqn. (9)[29]	—	—	0(0)	0(0)	0(0)	0(0)	0(0)	0(0)	This work
Ln = Tb to Yb	$G'_iA_2^0\langle r^2\rangle$	eqn. (9)[29]	—	—	0.057(3)	0.035(2)	0.052(3)	0.060(3)	0.047(2)	0.24(1)	This work

			Tridentate binding units									
			H^9	H^{10}	H^{11}	H^{12}	H^{13}	H^{14}	Me^3	Me^4	Me^5	Ref.
$[LnCo^{III}L_3]^{6+}$	F'_i	eqns. (4), (5)[30]	−0.07(3)	−0.01(1)	0.12(1)	0.24(1)	0.09(2)	0.17(1)	0.00(1)	−0.02(2)	0.00(2)	23
Ln = Ce to Eu	$G'_iA_2^0\langle r^2\rangle$	eqns. (4), (5)[30]	0.93(3)	0.067(4)	−0.019(6)	−0.33(1)	−0.23(1)	−0.15(1)	−0.149(2)	0.33(2)	−0.09(2)	23
$[LnCo^{III}L_3]^{6+}$	F'_i	eqns. (4), (5)[30]	0.79(4)	0.06(1)	0.09(1)	−0.11(3)	0.06(2)	−0.02(3)	−0.16(1)	0.29(3)	−0.04(2)	23
Ln = Tb to Yb	$G'_iA_2^0\langle r^2\rangle$	eqns. (4), (5)[30]	0.58(1)	0.038(2)	−0.007(3)	−0.20(1)	−0.132(8)	−0.097(9)	−0.096(5)	0.20(1)	−0.041(7)	23
$[LnCo^{III}L_3]^{6+}$	F'_i	eqn. (9)[29]	0.03(7)	0(0)	0.11(2)	0.15(3)	0.11(3)	0.05(3)	—	—	—	This work
Ln = Ce to Eu	$G'_iA_2^0\langle r^2\rangle$	eqn. (9)[29]	1.08(2)	0.068(3)	−0.021(3)	−0.402(9)	−0.249(6)	−0.206(4)	—	—	—	This work
$[LnCo^{III}L_3]^{6+}$	F'_i	eqn. (9)[29]	0.07(6)	0(0)	0.10(2)	0.11(3)	0.08(3)	0.07(2)	—	—	—	This work
Ln = Tb to Yb	$G'_iA_2^0\langle r^2\rangle$	eqn. (9)[29]	0.62(2)	0.036(1)	−0.120(3)	−0.234(6)	−0.145(3)	−0.120(3)	—	—	—	This work
$[LnCo^{II}L_3]^{5+}$	F'_i	eqns. (4), (5)[30]	−0.11(5)	−0.03(1)	0.10(1)	0.24(2)	0.09(2)	0.17(1)	0.06(2)	0.02(2)	−0.06(3)	This work
Ln = Ce to Eu	$G'_iA_2^0\langle r^2\rangle$	eqns. (4), (5)[30]	0.94(4)	0.080(7)	0.001(6)	−0.35(1)	−0.24(2)	−0.16(1)	−0.16(1)	−0.11(2)	0.38(3)	This work
$[LnCo^{II}L_3]^{5+}$	F'_i	eqns. (4), (5)[30]	0.76(6)	0.05(1)	0.10(1)	0.02(1)	0.08(3)	0.06(3)	−0.16(2)	−0.06(2)	0.31(4)	This work
Ln = Tb to Yb	$G'_iA_2^0\langle r^2\rangle$	eqns. (4), (5)[30]	0.64(2)	0.041(2)	−0.001(2)	−0.276(5)	−0.20(1)	−0.133(9)	−0.109(6)	−0.038(6)	0.24(1)	This work
$[LnCo^{II}L_3]^{5+}$	F'_i	eqn. (9)[29]	1.1(1)	0(0)	0.0(4)	−0.2(6)	−0.1(5)	−0.1(5)	—	—	—	This work
Ln = Ce to Eu	$G'_iA_2^0\langle r^2\rangle$	eqn. (9)[29]	1.6(4)	0.09(6)	−0.03(5)	−0.6(2)	−0.4(1)	−0.31(7)	—	—	—	This work
$[LnCo^{II}L_3]^{5+}$	F'_i	eqn. (9)[29]	0.0(2)	0(0)	0.10(6)	0.36(8)	0.38(7)	0.17(6)	—	—	—	This work
Ln = Tb to Yb	$G'_iA_2^0\langle r^2\rangle$	eqn. (9)[29]	0.75(4)	0.044(2)	−0.015(1)	−0.28(1)	−0.174(9)	−0.144(7)	—	—	—	This work

[a] To separate contact and pseudo-contact contributions (see text).

Table 6 Ln^{III}–H^i distances (r_i/Å) and electronic relaxation times (τ_e/ps) for (HHH)-$[LnCo^{III}L_3]^{6+}$ (Ln = Tb or Tm) in CD_3CN (298 K)

	H^1	H^2	H^3	H^4	H^5	H^6	H^9	H^{10}	H^{11}	H^{12}	H^{13}	H^{14}
$r_i[TbCo^{III}L_3]^{6+\,a}$	13.0(7)	13.9(8)	12.2(7)	8.2(5)	8.6(6)	7.7(6)	[b]	[c]	7.6(6)	6.1(5)	6.9(5)	6.9(8)
$r_i[TmCo^{III}L_3]^{6+\,a}$	11.1(7)	9.5(9)	10(1)	8.2(6)	7.1(6)	7.3(7)	[b]	7.5(4)	7.0(5)	5.7(4)	6.2(4)	6.7(8)
$r_i[TbCo^{III}L_3]^{6+\,d}$	12.5(2)	12.0(5)	11.2(4)	7.5(3)	7.3(2)	6.7(2)	[b]	[c]	6.7(2)	5.4(2)	6.3(2)	5.3(3)
$\tau_e{}^d$	0.6(4)	0.6(5)	0.9(4)	0.5(2)	0.5(1)	0.4(2)	[b]	[c]	0.6(3)	0.4(3)	0.7(1)	0.2(2)
$r_i[LaCo^{III}L_3]^{6+\,e}$	11.50	12.28	10.56	8.37	7.42	6.67	3.82	7.55	7.13	5.65	6.37	5.57
$r_i[LuCo^{III}L_3]^{6+\,e}$	11.84	12.92	11.04	8.18	7.15	6.97	3.86	7.40	6.89	5.49	6.24	5.45

[a] Obtained according to eqn. (12) with H^4 as reference (r_{H^4} = 8.18 Å). [b] Too short to obtain reliable relaxation times. [c] Overlap with other signals (methyl and solvent). [d] Obtained according to eqn. (10) with τ_r = 200 ps. [e] Taken from the crystal structures of complexes **6** and **7**.

Table 7 Comparison of theoretical[26] and experimental values of the axial magnetic anisotropic susceptibility (C_j) for (HHH)-$[LnCo^kL_3]^{(3+k)+\,a}$

	(HHH)-$[LnCo^{III}L_3]^{6+}$		(HHH)-$[LnCo^{II}L_3]^{5+}$		
	$A_2^0\langle r^2\rangle C_jT^{-2}/T^2$/ppm Å^3	Scaled $C_j{}^b$	$A_2^0\langle r^2\rangle C_jT^{-2}/T^2$/ppm Å^3	Scaled $C_j{}^b$	Theory[26]
Ce	413(10)[c]	−5.2(1)	597(185)	−6(2)	−6.3
Pr	666(13)	−8.0(2)	866(196)	−10(2)	−11.0
Nd	300(8)	−3.8(1)	501(131)	−5.5(1.4)	−4.2
Eu	−342(9)	4.3(1)	−532(169)	6(2)	4.0
Tb	4518(92)	−91(2)	5330(126)	−94(3)	−86.0
Dy	4941(150)	−100(3)	5668(189)	−100(3)	−100.0
Ho	2660(44)	−53(1)	3258(143)	−57(3)	−39.0
Er	−562(18)	11.4(4)	−664(113)	12(2)	33.0
Tm	−1614(44)	32.7(9)	2107(54)	37(1)	53.0
Yb	−651(19)	13.2(4)	−764(81)	13(2)	22.0

[a] Ratios relative to Nd^{III} (C_j = −100) are given (see text). [b] Values corrected for crystal-field effects. [c] The quoted errors correspond to those found during the fitting process.

of its weak paramagnetism) gives six parameters for each lanthanide: the axial magnetic anisotropy $A_2^0\langle r^2\rangle C_j/T^2$ and five contact contributions for twelve experimental shifts (12 × 6 fits),[29] which are collected in ESI Tables S10 and S11 together with satisfactory Wilcott agreement factors[21] ($0.002 \leq AF_j \leq 0.06$). The two sets of fitted parameters corresponding to the respective use of (HHH)-$[LaCo^{III}L_3]^{6+}$ **6** or (HHH)-$[LuCo^{III}L_3]^{6+}$ **7** as structural models show only minor differences except for a slightly better agreement with the crystal structure of (HHH)-$[LuCo^{III}L_3]^{6+}$ which is less distorted from the ideal C_3 symmetry. Further calculations consider only the latter complex as structural model. F_i' are obtained from δ_{ij}^c according to eqn. (2) for each lanthanide and average values for Ln = Ce to Eu and Tb to Yb are collected in Table 5. We observe a qualitative good agreement with F_i' values obtained by structure independent hyperfine shift analysis methods (eqns. 4 and 5) which suggest very similar solution and solid state structures. Further geometrical informations can be gained from the axial magnetic anisotropies and we have scaled $A_2^0\langle r^2\rangle C_j/T^2$ to −100 for Ln = Dy in order to compare our values with the accessible relative theoretical values of C_j tabulated by Bleaney (Table 7).[26] The relative anisotropic parameters for Ln = Tb to Yb are obtained by direct proportions while those for Ce to Eu are corrected for their larger crystal field (factor 1.6). The correlation between experimental and theoretical values (agreement factor AF = 0.23) is far better than those previously reported (AF = 0.44)[21] for $[EuZnL_3]^{5+}$ [21] and confirms that the crystal structure of (HHH)-$[LnCo^{III}L_3]^{6+}$ can be considered as a suitable geometrical model for the structure of (HHH)-$[LnCo^{III}L_3]^{6+}$ (Ce to Yb) in acetonitrile. The similarity between the $G_i'A_2^0\langle r^2\rangle$ terms obtained by structure dependent (eqns. 9 and 3) and structure independent (eqns. 4 and 5, Table 5) confirms that the principal magnetic axis (z axis) coincides with the intermetallic axis in solution in agreement with the observed axial C_3 symmetry. Finally, non-linear least squares fits by eqn. 9 for which $A_2^0\langle r^2\rangle C_j/T^2$, θ_i, r_i are simultaneously varied (δ_{ij}^c are fixed and taken from structure independent methods) show only minor variations of θ_i, r_i and magnetic anisotropy to minimise the square of the error between calculated and experimental pseudo-contact contributions to the paramagnetic shift (ESI Tables S12, S13 and S14), but the final agreement factor between theoretical and experimental Bleaney coefficients (C_j) is slightly improved (AF = 0.20). For both fitting processes, (HHH)-$[ErCo^{III}L_3]^{6+}$ displays the largest discrepancies and agreement factors of 0.18 and 0.16 respectively are obtained when these data are removed from the calculations. We thus conclude that the crystal structure of the cation in **7** is a satisfying model for rationalising paramagnetic NMR data (relaxation, chemical shifts, magnetic anisotropies) and the dissolution of (HHH)-$[LnCo^{III}L_3]^{6+}$ in acetonitrile is associated with a slight increased flexibility and fluxionality which provides ideal C_3 symmetry on the NMR timescale.

Solution structure of (HHH)-$[LnCo^{II}L_3]^{5+}$ by paramagnetic NMR

The presence of two paramagnetic centres Co^{II} and Ln^{III} in the same podate (HHH)-$[LnCo^{II}L_3]^{5+}$ complicates the analysis of the paramagnetic ^1H NMR shifts and relaxation processes because (i) Co^{II} cannot be considered as a paramagnetic dot with negligible spin delocalisation, (ii) possible magnetic coupling between the metal ions affects relaxation processes and hyperfine constants as recently described by Bertini, Luchinat and co-workers[34,57] and (iii) the large magnetic moments in acetonitrile drastically broaden NMR signals and prevent detection of scalar or dipolar ^1H–^1H couplings. This latter limitation precludes any reliable assignments of ^1H NMR spectra for Ln = Tb to Yb and leads to considerable uncertainties for Ce to Eu. Consequently, no reliable separation of contact and pseudo-contact contributions and no test for isostructurality using structure independent techniques can be applied. In order to overcome this limitation, we have determined the experimental magnetic moments of (HHH)-$[LnCo^{II}L_3]^{5+}$ (Ln = La, Ce, Yb or Lu) in acetonitrile (233–333 K) using the Evans method modified by Piguet for supramolecular complexes.[58] All studied complexes display Curie behaviours with μ_{eff}^{LnCo} = 5.0(1) (Ln = La), 5.57(8) (Ln = Ce), 6.6(1) (Ln = Yb) and 4.93(8) μ_B (Ln = Lu). The magnetic moments for Ln = La

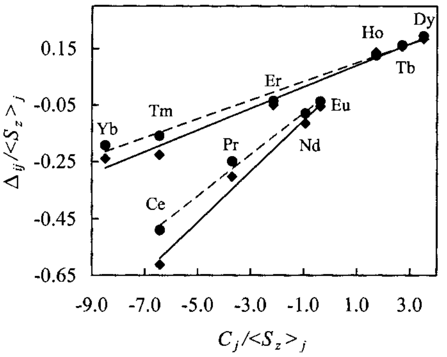

Fig. 7 Plot of $\Delta_{ij}/\langle S_z\rangle_j$ *vs.* $C_j/\langle S_z\rangle_j$ (eqn. 4) for H^{10} in $[LnCo^{III}L_3]^{6+}$ (●) and $[LnCo^{II}L_3]^{5+}$ (◆) (acetonitrile, 298 K).

or Lu are typical of monometallic pseudo-octahedral high-spin Co^{II} co-ordinated by three bidentate benzimidazole pyridine units ($\mu_{\text{eff}}^{\text{Co}} = 4.8(1)$ μ_B)[59] and we calculate $\mu_{\text{eff}}^{\text{Ce}} = 2.4(1)$ and $\mu_{\text{eff}}^{\text{Yb}} = 4.4(1)$ μ_B in (HHH)-$[LnCo^{II}L_3]^{5+}$ by using eqn. (17) for two magnetically uncoupled metal ions.[20]

$$\mu_{\text{eff}}^{\text{LnCo}} = \sqrt{(\mu_{\text{eff}}^{\text{Ln}})^2 + (\mu_{\text{eff}}^{\text{Co}})^2} \qquad (17)$$

These values are in line with those expected for the free ions $\mu_{\text{eff}}^{\text{Ce}} = 2.54$ and $\mu_{\text{eff}}^{\text{Yb}} = 4.54$ μ_B which implies that (i) each metal ion behaves as an independent paramagnetic centre in (HHH)-$[LnCo^{II}L_3]^{5+}$ and (ii) the methylene spacer acts as an insulator preventing spin delocalisation between the binding sites. The observed chemical shifts $\delta_{ij}^{\text{LnCo}}$ are thus given by eqns. (18) and (19) for (HHH)-$[LnCo^{II}L_3]^{5+}$ and (HHH)-

$$\delta_{ij}^{\text{LnCo}^{\text{II}}} = \delta_i^{\text{LaCo}^{\text{II}}} + \Delta_{ij}^{\text{Ln}}(\text{Co}^{\text{II}}) \qquad (18)$$

$$\delta_{ij}^{\text{LnCo}^{\text{III}}} = \delta_i^{\text{LaCo}^{\text{III}}} + \Delta_{ij}^{\text{Ln}}(\text{Co}^{\text{III}}) \qquad (19)$$

$[LnCo^{III}L_3]^{6+}$ respectively in which $\Delta_{ij}^{\text{Ln}}(\text{Co}^k)$ is the isotropic paramagnetic shift induced at nucleus *i* by the lanthanide *j* in the complexes containing Co^k in the non-covalent tripod. Since the two paramagnetic centres are magnetically independent and if we assume that the structures of (HHH)-$[LnCo^kL_3]^{(3+k)+}$ ($k = 2$ or 3) are similar, the approximation $\Delta_{ij}^{\text{Ln}}(\text{Co}^{\text{II}}) \cong \Delta_{ij}^{\text{Ln}}(\text{Co}^{\text{III}})$ holds, and combination of eqns. (18) and (19) gives (20) which

$$\delta_{ij}^{\text{LnCo}^{\text{II}}} = (\delta_i^{\text{LaCo}^{\text{II}}} - \delta_i^{\text{LaCo}^{\text{III}}}) + \delta_{ij}^{\text{LnCo}^{\text{III}}} \qquad (20)$$

allows some predictions for the ^1H NMR spectra of (HHH)-$[LnCo^{II}L_3]^{5+}$ from those of (HHH)-$[LaCo^{II}L_3]^{5+}$, (HHH)-$[LaCo^{III}L_3]^{6+}$ and (HHH)-$[LnCo^{III}L_3]^{6+}$ for which reliable assignments are accessible (ESI Table S6). The calculated shifts of $\delta_{ij}^{\text{LnCo}^{\text{II}}}$ are very close to the experimental values leading to reliable assignments of the ^1H NMR spectra for the complete lanthanide series (Table 1). Application of the structurally independent, but crystal-field dependent analysis (eqns. 4 and 5) to the experimental lanthanide-induced paramagnetic shifts $\Delta_{ij}^{\text{Ln}}(\text{Co}^{\text{II}})$ provides very similar trends to those previously described for $\Delta_{ij}^{\text{Ln}}(\text{Co}^{\text{III}})$ (systematic breaks around Tb, Fig. 7) and leads to comparable sets of F_i' and $G_i'A_2^0\langle r^2\rangle$ values (Table 5). For H^{1-4}, the paramagnetic shifts are mainly influenced by the close Co^{II} and the weak effect of the remote Ln^{III} becomes comparable with linewidth leading to large uncertainties.

Application of the structure and crystal-field independent hyperfine shift analysis method (eqn. 6) to $\Delta_{ij}^{\text{Ln}}(\text{Co}^{\text{II}})$ systematically produces straight lines along the complete lanthanide series thus establishing a single structure in solution and attributing the breaks of eqns. (4) and (5) to a change of the crystal-field parameters $A_2^0\langle r^2\rangle_{\text{Ln=Ce–Eu}}/A_2^0\langle r^2\rangle_{\text{Ln=Tb–Yb}} = 1.6(3)$ in (HHH)-$[LaCo^{II}L_3]^{5+}$ which is identical, within experimental error, to that found for (HHH)-$[LaCo^{III}L_3]^{6+}$ (ESI Fig. S4). The associated structural R_{ik} factors (eqn. 7) and intercepts $F_i' - F_k'R_{ik}$ (eqn. 6) are collected in ESI Table S15 and are comparable to those found for (HHH)-$[LaCo^{III}L_3]^{6+}$ as demonstrated by the approximate straight line (slope = 1.03; correlation coefficient $R^2 = 0.9482$) between $R_{ik}^{\text{LnCo}^{\text{III}}}$ and $R_{ik}^{\text{LnCo}^{\text{II}}}$ for each pair of protons (Fig. 8). Pairs involving H^{11} have been removed because of the special location of this proton close to the magic angle (54.74°) which makes them excessively sensitive to minor changes.[19] The observed good correlation points to very similar structures in solution when going from (HHH)-$[LaCo^{III}L_3]^{6+}$ to (HHH)-$[LaCo^{II}L_3]^{5+}$. It is worth noting that the larger discrepancies involve protons belonging to the bidentate binding units because (i) it is the portion of the podate which is the most affected by the $Co^{II/III}$ oxidation for which we expect a contraction of 0.19 Å in the Co–N bond distances[60] and (ii) $\Delta_{ij}^{\text{Ln}}(\text{Co}^{\text{II}})$ is small and dominated by the paramagnetism of Co^{II}. Application of the structure dependent Kemple method (eqn. 9) using the crystal structure of (HHH)-$[LuCo^{III}L_3]^{6+}$ in **7** as model and multi-linear least-squares fit of the (HHH)-$[LnCo^{II}L_3]^{5+}$ NMR data (Ln = Ce to Yb) provides F_i' (Table 5) and axial magnetic anisotropies (Table 7) very similar to those found for the related $LnCo^{III}$ analogues in solutions, but with larger uncertainties. The agreement factor between the scaled experimental axial anisotropy corrected for crystal field effects and Bleaney's C_j coefficients amounts to $AF = 0.23$ (Table 7) which is identical to that found for (HHH)-$[LuCo^{III}L_3]^{6+}$. We conclude that both non-covalent podates with Co^{II} or Co^{III} in the non-covalent tripod possess similar C_3-symmetrical structures in solution for which the crystal structure of the cation in **7** is a satisfying model.

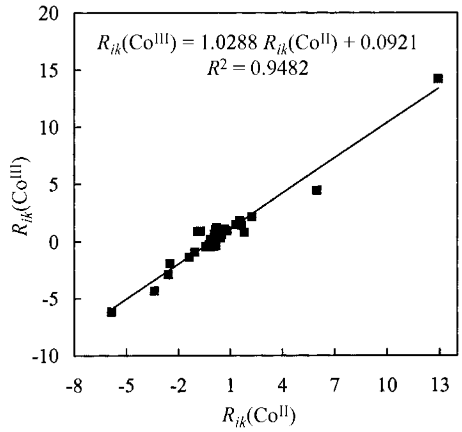

Fig. 8 Plot of $R_{ik}^{\text{LnCo}^{\text{III}}}$ *vs.* $R_{ik}^{\text{LnCo}^{\text{II}}}$ for pairs of protons (excluding H^{11}) in (HHH)-$[LnCo^mL_3]^{(3+m)+}$ ($m = 2$ or 3; CD_3CN, 298 K).

Conclusion

The quantitative self-assembly of the labile podates (HHH)-$[LnCo^{II}L_3]^{5+}$ demonstrates that the stereochemically demanding Co^{II} is compatible with its introduction into the pseudo-octahedral site of the non-covalent tripod. Compared to the flexible podates (HHH)-$[LnZnL_3]^{5+}$ containing spherical Zn^{II} (d^{10})[21] and the fast-exchanging spin-crossover Fe^{II} in (HHH)-$[LnFe^{II}L_3]^{5+}$,[20] the cobalt(II) tripods in (HHH)-$[LnCoL_3]^{5+}$ are expected to be geometrically more rigid thus imposing structural control over the neighbouring nine-co-ordinate lanthanide site. Oxidative post-modification to give inert Co^{III} (d^6 low spin) still increases rigidity and provides C_3-symmetrical podates (HHH)-$[LnCo^{III}L_3]^{6+}$ ideally suited for testing crystal-field dependent and independent paramagnetic NMR techniques in solution since we expect only minor changes between solid state structures accessible by X-ray diffraction techniques and solution structures. Moreover, the crystal structures of **6** and **7** show that no major geometrical variations occur along the complete lanthanide series in the solid state as a result of the rigidity of the triple-helical edifice.

This strongly contrasts with the paramagnetic NMR analyses of these complexes in solution which display systematic breaks around the middle of the lanthanide series (Ln = Tb) according to the classical structure independent, but crystal-field dependent Reilley method (eqns. 4 and 5). This suggests possible structural changes, but this counter-intuitive hypothesis is ruled out by application of the structure and crystal-field independent method of Geraldes (eqn. 6) which unambiguously establishes isostructurality along the complete lanthanide series for (HHH)-$[LnCo^{III}L_3]^{6+}$ and assigns breaks to concomitant variations of the crystal-field parameter and hyperfine coupling constants. A new strategy thus emerges for solving solution structures of lanthanide complexes by paramagnetic NMR.

(1) Isostructurality and prediction of NMR spectra for strongly paramagnetic complexes whose assignments are prevented by undetectable scalar or NOE effects are obtained by the two-nuclei Geraldes technique (eqn. 6).[23,32] Geometrical variations along the lanthanide series are easily detected by changes in R_{ik} values while electronic variations[32] are sometimes more difficult to establish due to compensation effects.[23]

(2) The same set of NMR data is then analysed according to Reilley's method (eqns. 4 and 5) which, combined with the prior knowledge of isostructural series, gives access (i) to the precise origin of the breaks (geometrical or crystal-field changes, variations of hyperfine coupling constants) and (ii) to the quantitative relative ratio of crystal-field parameters and hyperfine Fermi constants between the different series. For our rigid model system (HHH)-$[LnCo^{III}L_3]^{6+}$, a single isostructural series Ln = Ce to Yb is found with eqn. (6) but changes in hyperfine coupling constants escape detection with this technique. The subsequent analysis with eqns. (4) and (5) indeed demonstrates that concomitant abrupt variations of the crystal-field parameter and hyperfine coupling constants occur around Ln = Tb, an effect which is reminiscent of related anomalous physical and/or chemical behaviours occurring near the middle of the lanthanide series, sometimes referred to as the 'gadolinium break', and resulting from introduction of extra electrons into the half-filled 4f shell. Extensions towards closely related triple-stranded homodimetallic f–f helicates reach the same conclusions[18,19] which strongly suggest that further theoretical work is required to rationalise these electronic effects. Applications of points (1) and (2) to the precursor complexes (HHH)-$[LnCo^{II}L_3]^{5+}$ possessing two magnetically independent paramagnetic centres confirm our hypothesis that non-covalent cobalt(II) tripods are also rigid enough to control the lanthanide co-ordination sphere leading to a solution structure very close to that found for (HHH)-$[LnCo^{III}L_3]^{6+}$.

(3) The ultimate step of the structural analysis concerns the elucidation of the molecular geometry. Field-dependent paramagnetic relaxation processes (eqns. 10 and 11) depend on several parameters which are difficult to estimate (electronic τ_e and rotational τ_r correlation times for instance), but they provide rough Ln–nucleus distances without resorting to any structural model. The combination of these distances with magnetic anisotropies and structural factors resulting from the structure dependent hyperfine shift analysis methods of Kemple[29] or Forsberg *et al.*[35] (eqn. 9) allows a quantitative geometrical analysis justifying rejection, acceptance or adjustment of the proposed structural model. Again, application of these techniques to the rigid complexes (HHH)-$[LnCo^{III}L_3]^{6+}$ demonstrates that the solution structure closely matches the solid state structure except for minor changes associated with larger fluxionality in solution.

In conclusion, (HHH)-$[LnCo^{II}L_3]^{5+}$ and (HHH)-$[LnCo^{III}L_3]^{6+}$ are rigid enough to demonstrate the validity of this paramagnetic NMR approach while the latter is easier to analyse because Ln^{III} is the single paramagnetic centre. We suspect that previously reported conclusions involving structural changes and peculiar spin delocalisations in related axial systems such as (HHH)-$[LnZnL_3]^{5+}$,[21] dimetallic f–f triple-stranded helicates,[16,18,19] covalent podates[49] and monometallic triple helical complexes[41,61] based on the classical approach (eqns. 4 and 5) are doubtful and merit reconsideration.

Experimental

Solvents and starting materials

These were purchased from Fluka AG (Buchs, Switzerland) and used without further purification unless otherwise stated. The ligand 2-{6-[*N*,*N*-diethylcarbamoyl]-pyridin-2-yl}-1,1′-dimethyl-2′-(5-methylpyridin-2-yl)-5,5′-methylene-bis[1*H*-benzimidazole] (L) was prepared according to literature procedures,[21] the perchlorate salts $Ln(ClO_4)_3\cdot nH_2O$ (Ln = La to Lu or Y) from the corresponding oxides (Glucydur, 99.99%).[62] $Co(ClO_4)_2\cdot 6H_2O$ was purchased from Aldrich.

Preparations

$LnCo^{II}$ complexes: $[LaCoL_3][ClO_4]_5\cdot 0.25C_4H_{10}O\cdot 1.5H_2O$ 1, $[YCoL_3][ClO_4]_5\cdot 0.5C_4H_{10}O\cdot 2H_2O$ 2 and $[LuCoL_3][ClO_4]_5\cdot 0.5C_4H_{10}O\cdot H_2O$ 3. A solution of 12.2 μmol of $Ln(ClO_4)_3\cdot nH_2O$ (Ln = La, Y or Lu) and 36.5 mg (12.2 μmol) of $Co(ClO_4)_2\cdot 6H_2O$ in acetonitrile (5 cm^3) was slowly added to a solution of L (20 mg, 36.3 μmol) in 1:1 CH_2Cl_2–CH_3CN (4 cm^3). After stirring 1 h at room temperature the solution was evaporated, the solid residue dried under vacuum and redissolved in CH_3CN (2 cm^3). Diethyl ether was diffused into the solution for 24 h. The resulting pale yellow microcrystalline aggregates were collected by filtration and dried to give 73–80% of the complexes (**1**, Found: C, 50.66; H, 4.44; N, 12.40. $C_{99}H_{99}Cl_5CoLaN_{21}O_{23}\cdot 0.25C_4H_{10}O\cdot 1.5H_2O$ requires C, 50.64; H, 4.44; N, 12.40%. **2**, Found: C, 51.76; H, 4.62; N, 12.53. $C_{99}H_{99}Cl_5CoN_{21}O_{23}Y\cdot 0.5C_4H_{10}O\cdot 2H_2O$ requires C, 51.12; H, 4.63; N, 12.52%. **3**, Found: C, 50.00; H, 4.41; N, 12.16. $C_{99}H_{99}Cl_5CoLuN_{21}O_{23}\cdot 0.5C_4H_{10}O\cdot H_2O$ requires C, 50.18; H, 4.41; N, 12.16%).

$LnCo^{III}$ complexes: $[LaCoL_3][ClO_4]_5Br\cdot 0.5H_2O$ 4 and $[LaCoL_3][ClO_4]_6\cdot 0.1C_4H_{10}O\cdot 2.4H_2O$ 5. 10 μl of bromine in acetonitrile (3.11 M, 65.4 μmol, 3 equivalents) were slowly added to a stirred solution of 50 mg of $[LaCoL_3][ClO_4]_5\cdot 0.25C_4H_{10}O\cdot 1.5H_2O$ **1** (21 μmol) in acetonitrile (1.75 cm^3). The solution was heated to 50 °C for 3 h, the solvent distilled off and the solid dried under vacuum for 3 h. The residue was dissolved in acetonitrile–water (2.1 cm^3 : 0.085 cm^3), the resulting solution filtered and diethyl ether slowly diffused for 24 h. The resulting orange microcrystalline powder was collected by filtration and dried to give 95% of complex **4** (Found: C, 48.63; H, 4.21; Br, 3.64; N, 12.22. $C_{99}H_{99}BrCl_5CoLaN_{21}O_{23}\cdot 0.5H_2O$ requires C, 49.23; H, 4.17; Br, 3.30; N, 12.18%). The bromide anion was replaced by ClO_4^- by treatment with $AgClO_4$ (1 equivalent) in acetonitrile. AgBr was carefully filtered twice over cellulose and diethyl ether slowly diffused to give 83% of complex **5** (Found: C, 47.89; H, 4.27; N, 11.91. $C_{99}H_{99}Cl_6CoLaN_{21}O_{27}\cdot 0.1C_4H_{10}O\cdot 2.4H_2O$ requires C, 48.21; H, 4.26; N, 11.87%). Slow diffusion of diisopropyl ether into a concentrated solution of **5** provided X-ray quality prisms of $[LaCoL_3][ClO_4]_{5.5}[OH]_{0.5}\cdot 4CH_3CN\cdot 2H_2O$ **6**,[22] but a similar procedure with Ln = Lu failed. Fragile orange X-ray quality prisms of $[LuCoL_3][CF_3SO_3]_6\cdot 2CH_3CN\cdot H_2O$ **7** were obtained when 30 equivalents of $NBu_4CF_3SO_3$ were added to the mother liquor prior to diffusion of diisopropyl ether. All these complexes gave IR spectra compatible with their formulations.

$[LnCoL_3][ClO_4]_5$ and $[LnCoL_3][ClO_4]_5Br$ (Ln = La to Lu or Y). These complexes were prepared *in situ* for ^1H NMR and magnetic studies. 280 μl (5.6 μmol) of an equimolar 0.12 M solution of $Ln(ClO_4)_3\cdot nH_2O$ (Ln = La to Lu or Y) and $Co(ClO_4)_2\cdot 6H_2O$ in acetonitrile was added to L (9.1 mg, 16.8 μmol) dissolved in dichloromethane–acetonitrile (1:1, 4 cm^3)

under an inert atmosphere. After evaporation of the solution, the solid residue was dried under vacuum, then dissolved in 700 μl of degassed CD$_3$CN to give 8 mmol dm^{-3} [LnCoL$_3$][ClO$_4$]$_5$ (Ln = La to Lu or Y) whose purity was checked by ^{1}H NMR spectroscopy. Addition of bromine (16.8 μmol, 3 equivalents) followed by warming at 50 °C for 3 h quantitatively oxidised Co^{II} to Co^{III}. The solvent was evaporated, the complexes [LnCoL$_3$][ClO$_4$]$_5$Br (Ln = La to Lu or Y) were dried under vacuum, redissolved in degassed CD$_3$CN (700 μl) and used for NMR measurements.

CAUTION: perchlorate salts with organic ligands are potentially explosive and should be handled with the necessary precautions.[63]

Crystal-structure determination of [LuCoL$_3$][CF$_3$SO$_3$]$_6$·2CH$_3$CN·H$_2$O 7

C$_{109}$H$_{107}$CoF$_{18}$LuN$_{23}$O$_{22}$S$_6$, M = 2859.4, monoclinic, space group $P2_1/c$, a = 21.949(4), b = 20.864(4), c = 25.809(5) Å, β = 95.61(3)°, U = 11762(4) Å^3, Z = 4, μ(Mo-Kα) = 1.18 mm^{-1}, T = 190 K. 18944 Unique reflections (R_{int} for equivalent reflections = 0.078) of which 12926 were observable [$|F_o| > 4\sigma(F_o)$]. Data were corrected for Lorentz and polarisation effects. The structure was solved by direct methods using MULTAN 87;[64] all other calculations used XTAL[65] and ORTEP II.[47] Full-matrix least-squares refinement based on F gave final values R = 0.061, wR = 0.063 for 1593 variables and 12926 contributing reflections. The ethyl group C29a–C30a displayed a cross disorder, which was refined with four atomic sites and population parameters of 0.6 and 0.4. A second ethyl group C27b–C28b exhibited a slightly distorted geometry, but no splitting of the atomic sites could be refined. Two triflate anions (h and i) were disordered and refined with 14 and 13 atomic sites respectively. The disordered atomic sites were refined with isotropic displacement parameters (31 atoms) and all other non-H atoms (163) were refined with anisotropic displacement parameters. The H atoms were placed in calculated positions and contributed to F_c calculations.

CCDC reference number 186/2250.

See http://www.rsc.org/suppdata/dt/b0/b007219m/ for crystallographic files in .cif format.

Physical measurements

Electronic spectra in the UV-Vis region were recorded at 20 °C from 10^{-4} M solutions in MeCN with a Perkin-Elmer Lambda 900 spectrometer using quartz cells of 0.1 and 0.01 cm path length. Spectrophotometric titrations were made under and N$_2$ atmosphere using Hellma optrodes (optical path length 0.1 cm) immersed in the thermostatted titration vessel and connected to a J&M diode array spectrometer (Tidas series). In a typical experiment, 50 cm^3 of L in acetonitrile (10^{-4} M) were titrated at 20 °C with an equimolar solution of Ln(ClO$_4$)$_3$·nH$_2$O and Co(ClO$_4$)$_2$·6H$_2$O 1.00 mM in acetonitrile. After each addition of 0.20 ml the absorbances were recorded using the optrode and transferred to the computer. Mathematical treatment of the spectrophotometric titrations was performed with factor analysis[66] and the SPECFIT program.[42] IR spectra were obtained from KBr pellets with a Perkin-Elmer 883 spectrometer, ^{1}H NMR spectra at 25 °C on Varian and Bruker spectrometers at 200, 300, 400, 500 and 600 MHz. Chemical shifts are given in ppm with respect to TMS. The determination of longitudinal relaxation times (T_1) used the inversion-recovery technique. Pneumatically assisted electrospray (ESI-MS) mass spectra were recorded from 10^{-4} M acetonitrile solutions in API III and API 365 tandem mass spectrometers (PE Sciex) by infusion at 4–10 μl min^{-1}. The spectra were recorded under low up-front declustering or collision induced dissociation (CID) conditions, typically ΔV = 0–30 V between the orifice and the first quadrupole of the spectrometer. Determination of the total charge (z) of the complexes was made by using the isotopic pattern ($z \leqslant 3$) or adduct ions with perchlorate anions ($z > 3$).[67] Cyclic voltammograms were recorded using a BAS CV-50W potentiostat connected to a personal computer. A three-electrode system consisting of a stationary platinum disk working electrode, a platinum counter electrode and a non-aqueous Ag–AgCl reference electrode was used. NBu$_4$PF$_6$ (0.1 M in MeCN) served as an inert electrolyte. The reference potential ($E°$ = 0.12 V *vs.* SCE) was standardised against [Ru(bipy)$_3$](ClO$_4$)$_2$ (bipy = 2,2′-bipyridyl).[68] The scan speed was 100 mV s^{-1} and voltammograms were analyzed according to established procedures.[68] Magnetic data for samples in acetonitrile were obtained by the Evans' method adapted for superconducting magnets and supramolecular assemblies and using a Varian Gemini 300 spectrometer.[58] A complete description of the set-up and related calculations can be found in reference 20. Elemental analyses were performed by Dr H. Eder from the microchemical Laboratory of the University of Geneva.

Acknowledgements

We are grateful to Professor T. Jenny (University of Fribourg), Dr D. Jeannerat, Mr J.-P. Saulnier and Mr A. Pinto (University of Geneva) for recording NMR spectra at 200, 400, 500 and 600 MHz and to Professor C. Luchinat (University of Firenze) for helpful discussions. This work is supported through grants from the Swiss National Science Foundation.

References

1 J.-M. Lehn, *Supramolecular Chemistry*, VCH, Weinheim, New York, Basel, Cambridge, Tokyo, 1995; A. F. Williams, C. Piguet and R. Carina, *Transition Metals in Supramolecular Chemistry*, 1994, **448**, 409; D. Philps and J. F. Stoddart, *Angew. Chem., Int. Ed. Engl.*, 1996, **35**, 1154; S. Leininger, B. Olenyuk and P. J. Stang, *Chem. Rev.*, 2000, **100**, 853; C. Piguet, *J. Inclusion Phenom. Macrocycl. Chem.*, 1999, **34**, 361.

2 J.-M. Lehn, *Chem. Eur. J.*, 1999, **5**, 2455.

3 C. Piguet, G. Bernardinelli and G. Hopfgartner, *Chem. Rev.*, 1997, **97**, 2005 and references therein; E. C. Constable in *Comprehensive Supramolecular Chemistry*, eds. J. L. Atwood, J. E. D. Davies, D. D. MacNicol and F. Vögtle, Pergamon, Oxford, 1996, ch. 6.

4 A. M. Garcia, F. J. Romero-Salguero, D. Bassani, J.-M. Lehn, G. Baum and D. Fenske, *Chem. Eur. J.*, 1999, **5**, 1803 and references therein.

5 F. M. Raymo and J. F. Stoddart, *Curr. Opin. Colloid Interface Sci.*, 1998, **3**, 150 and references therein; M. Fujita and K. Ogura, *Coord. Chem. Rev.*, 1996, **148**, 249.

6 G. A. Breault, C. A. Hunter and P. C. Mayers, *Tetrahedron*, 1999, **55**, 5265; F. M. Raymo and J. F. Stoddart, *Chem. Rev.*, 1999, **99**, 1643.

7 V. L. Pecoraro, A. J. Stemmler, B. R. Gibney, J. L. Bodwin, H. Wang, J. W. Kampf and A. Barwinski, *Prog. Inorg. Chem.*, 1997, **45**, 83.

8 D. L. Caulder and K. N. Raymond, *J. Chem. Soc., Dalton Trans.*, 1999, 1185; D. L. Caulder and K. N. Raymond, *Acc. Chem. Res.*, 1999, **32**, 975; D. P. Funeriu, J.-M. Lehn, K. M. Fromm and D. Fenske, *Chem. Eur. J.*, 2000, **6**, 2103.

9 P. N. W. Baxter, J.-M. Lehn, A. DeCian and J. Fischer, *Angew. Chem., Int. Ed. Engl.*, 1993, **32**, 69.

10 F. Basolo, J. Chatt, H. B. Gray, R. G. Pearson and B. L. Shaw, *J. Chem. Soc. A*, 1971, 2207; S. F. Lincoln and A. E. Merbach, *Adv. Inorg. Chem.*, 1995, **42**, 1 and references therein.

11 C. Piguet and J.-C. G. Bünzli, *Chem. Soc. Rev.*, 1999, **28**, 347.

12 X. Y. Wang, T. Z. Lin, V. Comblin, A. Lopez-Mut, E. Merciny and J. F. Desreux, *Inorg. Chem.*, 1992, **31**, 1095.

13 V. Comblin, D. Gilsoul, M. Hermann, V. Humblet, V. Jacques, M. Mesbahi, C. Sauvage and J. F. Desreux, *Coord. Chem. Rev.*, 1999, **185–186**, 451 and references therein; D. Parker, P. K. Senanayake and J. A. G. Williams, *J. Chem. Soc., Perkin Trans. 2*, 1998, 2129; P.-A. Pittet, D. Früh, V. Tissière and J.-C. G. Bünzli, *J. Chem. Soc., Dalton Trans.*, 1997, 895.

14 P. Caravan, J. J. Ellison, T. J. McMurry and R. B. Lauffer, *Chem. Rev.*, 1999, **99**, 2293; M. P. Lowe and D. Parker, *Chem. Commun.*, 2000, 707.

15 I. Ramade, O. Kahn, Y. Jeannin and F. Robert, *Inorg. Chem.*, 1997, **36**, 930; M. L. Kahn, C. Mathonière and O. Kahn, *Inorg. Chem.*, 1999, **38**, 3692; J.-P. Costes, F. Dahan, A. Dupuis and J.-P. Laurent, *Inorg. Chem.*, 1996, **35**, 2400; J.-P. Costes, F. Dahan, A. Dupuis and

J.-P. Laurent, *Inorg. Chem.*, 1997, **36**, 3429; J.-P. Costes, F. Dahan, A. Dupuis and J.-P. Laurent, *Chem. Eur. J.*, 1998, **4**, 1616; J.-P. Costes, F. Dahan and A. Dupuis, *Inorg. Chem.*, 2000, **39**, 165; S. J. Archibald, A. J. Blake, S. Parsons, M. Schröder and R. E. P. Winpenny, *J. Chem. Soc., Dalton Trans.*, 1997, 173; E. K. Brechin, S. G. Harris, S. Parsons and R. E. P. Winpenny, *J. Chem. Soc., Dalton Trans.*, 1997, 1665.

16 (*a*) C. Piguet, J.-C. G. Bünzli, G. Bernardinelli, G. Hopfgartner and A. F. Williams, *J. Am. Chem. Soc.*, 1993, **115**, 8197; (*b*) N. Martin, J.-C. G. Bünzli, V. McKee, C. Piguet and G. Hopfgartner, *Inorg. Chem.*, 1998, **37**, 577; (*c*) M. Elhabiri, R. Scopelliti, J.-C. G. Bünzli and C. Piguet, *J. Am. Chem. Soc.*, 1999, **121**, 10747.

17 C. F. G. C. Geraldes, in *NMR in Supramolecular Chemistry*, ed. M. Pons, Kluwer Academic, Amsterdam, 1999, p. 133 and references therein; J. A. Peters, *J. Magn. Reson.*, 1986, **68**, 240.

18 C. Platas, M. Elhabiri, M. Hollenstein, J.-C. G. Bünzli and C. Piguet, *J. Chem. Soc., Dalton Trans.*, 2000, 2031.

19 S. Rigault, C. Piguet and J.-C. G. Bünzli, *J. Chem. Soc., Dalton Trans.*, 2000, 2045.

20 C. Piguet, E. Rivara-Minten, G. Bernardinelli, J.-C. G. Bünzli and G. Hopfgartner, *J. Chem. Soc., Dalton Trans.*, 1997, 421; C. Edder, C. Piguet, G. Bernardinelli, J. Mareda, C. G. Bochet, J.-C. G. Bünzli and G. Hopfgartner, *Inorg. Chem.*, 2000, **39**, 5059.

21 C. Piguet, J.-C. G. Bünzli, G. Bernardinelli, G. Hopfgartner, S. Petoud and O. Schaad, *J. Am. Chem. Soc.*, 1996, **118**, 6681.

22 S. Rigault, C. Piguet, G. Bernardinelli and G. Hopfgartner, *Angew. Chem., Int. Ed.*, 1998, **37**, 169.

23 S. Rigault and C. Piguet, *J. Am. Chem. Soc.*, 2000, **122**, 9304.

24 J. M. Briggs, G. P. Moss, E. W. Randall and K. D. Sales, *Chem. Commun.*, 1972, 1180.

25 R. M. Golding and M. P. Halton, *Aust. J. Chem.*, 1972, **25**, 2577.

26 B. J. Bleaney, *J. Magn. Reson.*, 1972, **8**, 91; J. Reuben and G. A. Elgavish, *J. Magn. Reson.*, 1980, **39**, 421.

27 B. R. McGarvey, *J. Magn. Reson.*, 1979, **33**, 445.

28 C. N. Reilley, B. W. Good and R. D. Allendoerfer, *Anal. Chem.*, 1976, **48**, 1446.

29 M. D. Kemple, B. D. Ray, K. B. Lipkowitz, F. G. Prendergast and B. D. N. Rao, *J. Am. Chem. Soc.*, 1988, **110**, 8275.

30 For reviews, see A. D. Sherry and C. F. G. C. Geraldes, in *Lanthanide Probes in Life, Chemical and Earth Sciences*, eds. J.-C. G. Bünzli and G. R. Choppin, Elsevier, Amsterdam, 1989, ch 4; J. A. Peters, J. Huskens and D. J. Raber, *Prog. NMR Spectrosc.*, 1996, **28**, 283; S. P. Babailov and Y. G. Krieger, *J. Struct. Chem.*, 1998, **39**, 580.

31 J. Ren and A. D. Sherry, *J. Magn. Reson.*, 1996, **B111**, 178.

32 C. Platas, F. Avecilla, A. de Blas, C. F. G. C. Geraldes, T. Rodriguez-Blas, H. Adams and J. Mahia, *Inorg. Chem.*, 1999, **38**, 3190.

33 J. Reuben, *J. Magn. Reson.*, 1982, **50**, 233.

34 M. Allegrozzi, I. Bertini, M. B. L. Janik, Y.-M. Lee, G. Liu and C. Luchinat, *J. Am. Chem. Soc.*, 2000, **122**, 4154; I. Bertini and C. Luchinat, *Coord. Chem. Rev.*, 1996, **150**, 1.

35 J. H. Forsberg, R. M. Delaney, Q. Zhao, G. Harakas and R. Chandran, *Inorg. Chem.*, 1995, **34**, 3705.

36 S. Aime, L. Barbero, M. Botta and G. Ermondi, *J. Chem. Soc., Dalton Trans.*, 1992, 225.

37 R. E. Wasylishen, in *NMR Spectroscopy*, eds. C. Dybowsky and R. L. Lichters, Dekker, New York, Basel, 1987, pp. 45–91.

38 P. D. Burns and G. N. LaMar, *J. Magn. Reson.*, 1982, **46**, 61.

39 I. Bertini, O. Galas, C. Luchinat and G. Parigi, *J. Magn. Reson.*, 1995, **113**, 151; R. Ruloff, R. N. Muller, D. Pubanz and A. E. Merbach, *Inorg. Chim. Acta*, 1998, **275–276**, 15; E. Toth, L. Helm, A. E. Merbach, R. Hedinger, K. Hegetschweiler and A. Janossy, *Inorg. Chem.*, 1998, **37**, 4104.

40 J. M. Brink, R. A. Rose and R. C. Holz, *Inorg. Chem.*, 1996, **35**, 2878.

41 F. Renaud, C. Piguet, G. Bernardinelli, J.-C. G. Bünzli and G. Hopfgartner, *Chem. Eur. J.*, 1997, **3**, 1646.

42 H. Gampp, M. Maeder, C. J. Meyer and A. D. Zuberbühler, *Talanta*, 1985, **32**, 95.

43 S. Margel, W. Smith and F. C. Anson, *J. Electrochem. Soc.*, 1978, **125**, 241.

44 C. Piguet, G. Bernardinelli, B. Bocquet, O. Schaad and A. F. Williams, *Inorg. Chem.*, 1994, **33**, 4112.

45 B. R. Serr, K. A. Andersen, C. M. Elliott and O. P. Anderson, *Inorg. Chem.*, 1988, **27**, 4499; S. Ferrere and C. M. Elliott, *Inorg. Chem.*, 1995, **34**, 5818; C. M. Elliott, D. L. Derr, S. Ferrere, M. D. Newton and Y.-P. Liu, *J. Am. Chem. Soc.*, 1996, **118**, 5221.

46 R. D. Shannon, *Acta Crystallogr., Sect. A*, 1976, **32**, 751.

47 C. K. Johnson, ORTEP II; Report ORNL-5138, Oak Ridge National Laboratory, Oak Ridge, TN, 1976.

48 J. H. Brewster, *Top. Curr. Chem.*, 1974, **47**, 29.

49 For a detailed derivation and discussion of P_{ij}, see F. Renaud, C. Piguet, G. Bernardinelli, J.-C. G. Bünzli and G. Hopfgartner, *J. Am. Chem. Soc.*, 1999, **121**, 9326.

50 C. Piguet, J.-C. G. Bünzli, G. Bernardinelli, C. G. Bochet and P. Froidevaux, *J. Chem. Soc., Dalton Trans.*, 1995, 83.

51 A. G. Orpen, L. Brammer, F. H. Allen, O. Kennard, D. G. Watson and R. Taylor, *J. Chem. Soc., Dalton Trans.*, 1989, S1.

52 L. J. Charbonnière, G. Bernardinelli, C. Piguet, A. M. Sargeson and A. F. Williams, *J. Chem. Soc., Chem. Commun.*, 1994, 1419.

53 I. Bertini, Golden Jubilee Lecture, 34th ICCC, Edinburgh, July 2000.

54 I. Bertini, F. Capozzi, C. Luchinat, G. Nicastro and Z. Xia, *J. Phys. Chem.*, 1993, **97**, 6351.

55 H. D. Powell, O. M. Ni Dhubhghaill, D. Pubanz, Y. Lebedev, W. Schlaepfer and A. E. Merbach, *J. Am. Chem. Soc.*, 1996, **118**, 9333.

56 A. Arduini, V. Böhmer, L. Delmau, J.-F. Desreux, J.-F. Dozol, M. A. Garcia Carrera, B. Lambert, C. Musigmann, A. Pochini, A. Shivanyuk and F. Ugozzoli, *Chem. Eur. J.*, 2000, **6**, 2135.

57 V. Clementi and C. Luchinat, *Acc. Chem. Res.*, 1998, **31**, 351.

58 D. F. Evans, *J. Chem. Soc.*, 1959, 2003; D. F. Evans, G. V. Fazakerley and R. F. Phillips, *J. Chem. Soc. A*, 1971, 1931; C. Piguet, *J. Chem. Educ.*, 1997, **74**, 815.

59 L. J. Charbonnière, A. F. Williams, C. Piguet, G. Bernardinelli and E. Rivara-Minten, *Chem. Eur. J.*, 1998, **4**, 485.

60 B. S. Brunschwig, C. Creutz, D. H. Macartney, T. K. Sham and N. Sutin, *Faraday Discuss. Chem. Soc.*, 1982, **74**, 113; K. Yanagi, Y. Ohashi, Y. Sasada, Y. Kaizin and H. Kobayashi, *Bull. Chem. Soc. Jpn.*, 1981, **54**, 118.

61 S. Petoud, J.-C. G. Bünzli, F. Renaud, C. Piguet, K. J. Schenk and G. Hopfgartner, *Inorg. Chem.*, 1997, **36**, 5750.

62 J. F. Desreux, in *Lanthanide Probes in Life, Chemical and Earth Sciences*, eds. J.-C. G. Bünzli and G. R. Choppin, Elsevier Publishing Co., Amsterdam, 1989, ch. 2, p. 43.

63 W. C. Wolsey, *J. Chem. Educ.* 1973, **50**, A335.

64 P. Main, S. J. Fiske, S. E. Hull, J. Lessinger, D. Germain, J.-P. Declercq and M. M. Woolfson, MULTAN 87, Universities of York and Louvain-La-Neuve, 1987.

65 XTAL 3.2 User's Manual, eds. S. R. Hall and J. M. Stewart, Universities of Western Australia and Maryland, 1989.

66 E. R. Malinowski and D. G. Howery, *Factor Analysis in Chemistry*, Wiley, New York, Chichester, 1980.

67 G. Hopfgartner, C. Piguet and J. D. Henion, *J. Am. Soc. Mass Spectrom.*, 1994, **5**, 748; G. Hopfgartner, F. Vilbois and C. Piguet, *Rapid Commun. Mass Spectrom.*, 1999, **13**, 302.

68 A. J. Bard and L. R. Faulkner, *Electrochemical Methods, Fundamentals and Applications*, Wiley, New York, Chichester, Brisbane, Toronto, Singapore, 1980.